TAMPERE UNIVERSITY OF TECHNOLOGY

Timo Saari

Electronic structure and spin polarization in Silicene nanostructures

Master's thesis

Examiner: Jouko Nieminen
Adviser: Hsin Lin
Examiners and topic approved by the Faculty Council of the Faculty of Natural Sciences on 5 June 2013

TIIVISTELMÄ

TAMPEREEN TEKNILLINEN YLIOPISTO
Teknis-luonnontieteellinen koulutusohjelma
SAARI, TIMO: Siliseeni-nanorakenteiden Elektronirakenne ja Spin-polarisaatio
Diplomityö, 58 sivua, 3 liitesivua
Elokuu 2013
Pääaine: Teknillinen fysiikka
Tarkastaja: Jouko Nieminen
Ohjaaja: Hsin Lin
Avainsanat: Siliseeni, tight-binding, Greenin funktio, spin-polarisaatio, kvantti-spin-Hall-ilmiö

Grafeenin ainutlaatuiset ominaisuudet ja mahdolliset sovelluskohteet ovat tehneet materiaalista nykyään hyvin tunnetun. Siliseeni on kuitenkin uudempi kokeellisestikin havaittu materiaali, jolla on samat hämmästyttävät ominaisuudet kuin grafeenilla. Lisäksi siliseenillä on kaksi huomattavaa etua grafeeniin verrattuna. Ensinnäkin vyöaukko siliseenissä on paljon suurempi kuin grafeenissa, mikä tekee siliseenistä houkuttelevamman materiaalin elektronisiin sovelluksiin. Toisekseen siliseeni on yhteensopiva nykyisten pii-perustaisten puolijohdeteollisuuden menetelmien kanssa.

Siliseenin elektronirakennetta on tässä työssä tutkittu tight-binding-menetelmällä sekä Greenin funktioilla. Erityisesti on keskitytty vyöaukkoon ja sen käyttäytymiseen sähkökentässä. Lisäksi on tutkittu paikallisia ilmiöitä zigzag-nauhoissa. Lopuksi nauhan keskelle on luotu keinotekoinen rajapinta sähkökentillä, jotka osoittavat eri suuntiin omissa nauhan puolikkaissaan.

Tulosten perusteella havaitaan, että siliseenin vyörakoa voidaan ulkoisesti säätää sähkökentällä. Sähkökentän kasvattaminen ensin pienentää aukkoa, kunnes se täysin sulkeutuu ja alkaa taas kasvaa. Vyöaukon helppo ja yksinkertainen manipulaatio avaa monia sovelluskohteita elektroniikassa.

Nanonauhoissa havaitaan kvantti-spin-Hall-ilmiö, sillä helikaaliset reunatilat asettuvat bulkkiaineen vyöaukkoon. Tämä viittaa siliseenin olevan topologinen eriste. Lisäksi siliseeninauhassa, johon on luotu rajapinta vastakkaisilla sähkökentillä, havaitaan tilojen paikallistumista rajapinnan läheisyyteen. Nämä rajapintatilat kulkevat vyöaukon yli ja niiden lokalisaatio voimistuu kasvavan sähkökentän myötä. Lisätutkimuksia tarvitaan esimerkiksi kokeilemalla erilaisia geometrioita tai lisäämällä magneettikenttä mukaan systeemiin.

ABSTRACT

TAMPERE UNIVERSITY OF TECHNOLOGY
Master's Degree Programme in Science and Engineering
SAARI, TIMO : Electronic Structure and Spin Polarization in Silicene Nanostructures
Master of Science Thesis, 58 pages, 3 Appendix pages
August 2013
Major: Advanced Engineering Physics
Examiner: Jouko Nieminen
Adviser: Hsin Lin
Keywords: Silicene, tight-binding, Green's function, spin-polarization, quantum spin Hall effect

Graphene is nowadays a famous material due to its exquisite properties and potential applications. However, silicene is more recent experimentally verified finding which possesses the same main features that make graphene interesting. Additionally silicene has two advantages over graphene. Firstly it has considerably larger band gap which is very important for electronic applications. Secondly silicene is much more suitable when it comes to actual applications with today's silicon-based semiconductor industry.

The electronic structure of silicene has been studied with tight-binding method supplemented by Green's function calculations. Concerning bulk silicene, the focus has been on the band gap and its manipulation with electric field. We have also studied nanoribbons where we have looked for localized effects at the edges. Furthermore an artificial interface has been created in the middle of the ribbon by applying opposite electric fields on the separate halves of the nanoribbon.

In summary, the results indicate that the band gap of silicene can be externally tuned with electric field. The gap becomes smaller until it completely closes by increasing the field. After this is starts to grow once more. Easy manipulation of the gap suggests a wide range of potential applications in electronics.

Nanoribbons exhibit quantum spin hall effect as there exist helical edge states in the bulk gap. In effect this suggests the topologically insulating nature of silicene. Furthermore, electric field interfaced silicene shows localization of states near the interface. These interface states cross the gap and their localization strengthens with increasing electric field. Not much can be said yet as further research is needed in the form of different geometries or application of magnetic field, for example.

PREFACE

Arriving at the subject of this thesis was more of a coincidence than strict intention. Originally silicene was to be a brief milestone in our quest to start studying three-dimensional topological insulators. Instead, silicene turned out to be an intriguing subject in itself.

As such the project has provided challenges and we have pondered the models and results back and forth with each iteration leading to a "better" idea. As a result everything on the way didn't find its place in the thesis and some have been reserved for possible future use. Despite this the thesis consists of the most central findings in silicene.

First of all I would like to thank my supervisor Jouko Nieminen for introducing me to the world of tight-binding. In addition, he's given me a hot topic to work on and presented valuable suggestions and ideas which made this thesis possible.

I would also like to offer my gratitude to Dr. Hsin Lin who often presented sound observations and viewed results with a critical eye. Without his help this thesis would look totally different especially when it comes to the last issue of the work, interfaced silicene nanoribbon.

13 August 2013

Timo Saari

CONTENTS

LIST OF SYMBOLS AND ABBREVIATIONS

GMR	Giant magnetoresistance
QSHE	Quantum spin Hall effect
SOC	Spin-orbit coupling
TB	Tight-binding
a	Lattice constant
$\mathbf{a}_1$, $\mathbf{a}_2$	Lattice vectors
$\mathbf{b}_1$, $\mathbf{b}_2$	Reciprocal lattice vectors
$\mathbf{B}$	Magnetic field
$B_{n,\mathbf{k}}$	Bloch sum
c	Speed of light
$c_{i\sigma}^{\dagger}$	Second quantization creation operator
$c_{i\sigma}$	Second quantization annihilation operator
c_n	Linear combination coefficient
$\mathbf{d}_{ij}$	Vector to next nearest neighbour
$\hat{\mathbf{d}}_{ij}$	Unit vector to next nearest neighbour
δ	Kronecker delta
Δ	Buckling parameter
e	Electron charge
E	Energy
$\mathbf{E}$	Electric field
$\epsilon_{\mathbf{k}}$	Electron energy in a solid
ε_n	Atomic orbital energy
ε_R	Rashba Hamiltonian matrix element
ε_{so}	SOC Hamiltonian matrix element

$\mathbf{F}$	Force
$\Psi_{\mathbf{k}}$	Crystal wave function
ϕ_n	Atomic orbital
G	Green's function
$\hbar$	Reduced Planck's constant
H	Hamiltonian
I	Identity matrix
$\mathbf{k}$	Wave vector
$\mathbf{L}$	Angular momentum operator
$L_{\pm}$	Ladder operators
λ_R	Rashba spin-orbit coupling strength
λ_{so}	Effective spin-orbit coupling strength
m	Electron mass
N	Total number of unit cells in the crystal
η	Imaginary parameter in Green's function
$\mathbf{p}$	Momentum
ρ	Density of states
$\mathbf{R}$	Lattice vector
S	Overlap matrix
$\mathbf{S}$	Spin operator
σ	Spin state
$\bar{\sigma}$	Vector of Pauli matrices
t	Hopping parameter
τ_i	Position of the i-th atom in the unit cell
$\mathbf{v}$	Velocity

V	Crystal potential
V'	Crystal potential due to all the atoms except the one at the origin
V_{at}	Atomic potential

1. INTRODUCTION

Both graphene and silicene have properties that make them very promising for spintronic applications. They are probably the most prominent materials in this area of research due to their superior characteristics. However, information processing through spin requires spin propagation over long distances which has been impossible so far. Graphene and silicene represent a breakthrough in this field. For example, spin relaxation length of 5 μm at room temperature in graphene was demonstrated by Gao et al. in IEEE International Electron Devices Meeting in 2012 [8]. This is the current record which greatly surpasses previous achievements. Moreover, a whopping relaxation length of over 100 μm is achieved when graphene is cooled near absolute zero [3].

In addition, these materials have other unique properties useful in spintronics. For instance, magnetic moments can be controlled in graphene when electrons condense around vacancies. By dissipating and condensing these electron clouds, the magnetic moments they carry can be switched on or off. This is the first time magnetization itself has been toggled rather than just reversing the direction of magnetization. [19].

This thesis attempts to shed light on the electronic structure of silicene in an easily comprehensible way. Hopefully the ideas and methods presented here are easily grasped by also those not familiar with condensed matter physics. As such we will recreate some former results with a deeper derivation than those found in publications and also devise something new of our own.

We are especially interested in two things that affect the main qualities of silicene. These are spin-orbit interaction and external electric field which have already been quite thoroughly studied despite the youth of the material. Still, this thesis should offer some valuable insight and new findings in this area of research.

In computational approach we have basically two alternatives to choose from in order to study silicene. These are the tight-binding method and *ab initio* calculations with density functional theory. We have chosen the former for its simplicity and ease of use. Furthermore, tight-binding method is also a good choice for possible future studies which may include more realistic configurations like the effect of substrate, impurities and defects among others. Tight-binding calculations will be complemented by Green's function formalism which allows for more expanded view and diverse possibilities.

First in chapter two we begin with an overview of silicene as a material along with its short history. Furthermore, as all research fundamentally aims for actual realizations and practical applications, we try to cover this topic as well to the extent that is possible. Next, chapters three and four cover the theoretical means that have made this thesis possible. In other words, tight-binding theory and Green's function formalism will be introduced and presented in such a manner that will help the reader form connections from theory to actual applications in future chapters.

Finally in chapters five and six we study bulk silicene and silicene nanoribbons, respectively. On top of this we present the theory of spin-orbit coupling and its relation to silicene in our attempt to study the interplay of electric field and this relativistic effect. Chapter five is heavily based on earlier work and results which will be derived in detail. Chapter six, on the contrary, will also put forth new information in the context of nanoribbon under inhomogeneous electric field.

2. THE PAST, PRESENT AND FUTURE OF SILICENE

Graphene is perhaps the most investigated material in the past decade due to its huge advantages over conventional materials in electronics industry. Novel, faster devices made from graphene have been proposed to replace their current counterparts. The main problems in realizing these dreams are the lack of controllable band gap and incompatibility with current silicon-based technology.

Since its recent discovery, silicene has been looked upon as the solution to these problems. Silicene, sharing the same important electronic properties as graphene, could be easily incorporated into present technology with the huge advantage of an appreciable naturally occurring band gap. In principle, graphene could be substituted with silicene wherever graphene is used. Therefore silicene can be considered as improved graphene.

This chapter is intended to give a general picture of silicene. The most important things to note are the properties that make silicene highly interesting for a broad range of applications. However, as a very new material all of silicene's possibilities have not yet been revealed. The most basic question – how to incorporate silicene's properties to practical solutions – is also open.

2.1 History

The history of silicene is short. This statement refers to the fact that silicene was experimentally observed only as recently as 2010 and extensive studies have been carried out in the past couple of years only. However, Takeda and Shiraishi [29] predicted silicene structure already in 1994. Despite this the term "silicene" was introduced by Guzmán-Verri and Lew Yan Voon in 2007 in their studies of silicon-based structures [11]. In addition there has been some speculation of one-atom thick silicon sheets for the past ten years. For example, Durgun et al. [5] studied silicon nanotubes and one-atom thick silicon sheets, or silicene as we now know it, using *ab initio* calculations in 2005. This is somewhat surprising given that the first one-atom thick material – graphene – was initially produced in 2004 by Geim and Novoselov and silicene was considered purely hypothetical. Naturally the discovery of graphene aroused much interest and led to a huge amount of studies fueled by graphene's huge potential as the next-generation electronic device material. Though

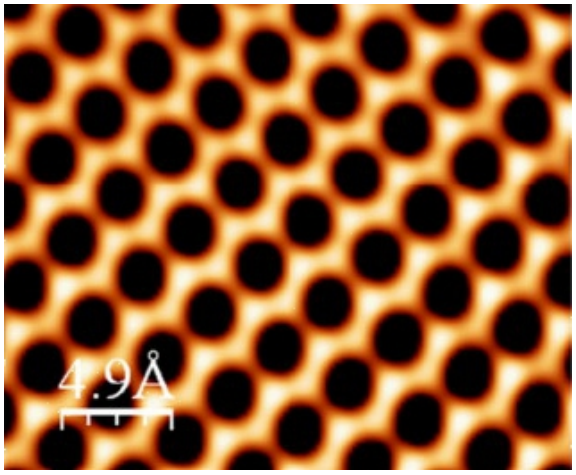

Figure 2.1: Silicene honeycomb structure on Ag(111). Adapted from reference [14].

graphene still remains a hot topic, silicene has started to take its place as the next wonder material. This can be attributed to its similar properties to graphene as well as its easier inclusion to current silicon-based technologies.

As previously mentioned, silicene was first synthetized in 2010 by Lalmi et al. [14]. Even though this was the first major breakthrough in producing a real silicene sheet, the honour of the discovery can be shared among Lalmi's group and Vogt's group. In 2012 Vogt et al. were able to synthetize silicene on Ag(111) surface in the same manner as Lalmi's group [34]. However, Vogt's silicene had arguably better quality since its Si-Si distance better matched values given by DFT calculations. Furthermore, Vogt et al. questioned Lalmi's results. They believed the STM images presented (figure 2.1) showed only clean Ag(111) surface mimicking silicene-like structure. In any case, these were only suspicions and both groups can be granted the honour of being the first to produce silicene on substrate.

Nowadays there has been a number of studies considering the electronic structure of silicene as well as silicene nanoribbons. Especially the means to tune the band gap is important for possible electronic applications and this has been studied by Drummond et al. [4] among others. Most studies are centered on the topic of single-layer silicene but multilayered structures have not been totally omitted. For example, Liu et al. investigated bilayer silicene and found it exhibiting a superconducting state [16]. Single-layer silicene has also been experimentally connected to superconductivity by Chen et al. with a critical temperature of 35–40 K [2]. This again was observed with Ag(111) as substrate. On top of all this, silicene has been connected to topological insulators which is a brand new field in material science. This shows how broad range of phenomena can be found in silicene and why it is an intriguing playing ground for both experimentalists and theorists alike.

2.2 Fabrication and substrates

Fabricating a single silicene sheet is a challenging task. Carbon can naturally form honeycomb structures through sp^2 hybridization and the result is known as graphene. Comparing this to silicon, sp^2 hybridization is not energetically favourable as sp^3 hybridized structures are more stable for silicon. This is the reason why graphene has been successfully made as an independent material in contrast to silicene. Despite this difficulty, freestanding silicene has been shown to be stable when a small buckling is introduced to the structure [13]. However, in practice silicene requires a substrate onto which it can grow. Attempts have been made to extract an independent silicene sheet but so far these have been in vain.

Forming silicene on Ag(111) surface can be done in ultrahigh vacuum conditions. First the silver surface is cleaned by a combination of sputtering and annealing. The second step involves heating a silicon wafer so that silicon is evaporated and then deposited onto the surface held at 250 °C. This is the method used by both aforementioned groups. Lalmi et al. also pointed out that the rate of deposition must be lower than 0.1 monolayers per minute.

Up till now only two other substrates have been found. The first one is (0001)-oriented thin film of zirconium diboride (ZrB_2) grown on silicon wafers which support the formation of silicene through surface segregation [7]. The other is (111)-oriented crystalline iridium as reported by Meng et al. [18].

The main problem with these three substrates is that they are conductors. As such they hide silicene's electrical properties and make it difficult to compare experimental data with theoretical predictions. What is worse, Ag(111) is unsuitable substrate as it destroys the Dirac cone found in silicene [35; 10]. With this in mind, a semiconducting or insulating substrate that preserves silicene's properties needs to be found. The best solution would of course be to make an independent sheet of silicene but so far no clear idea as how this could be done has been presented.

Even though no insulating substrates have been experimentally found, Liu et al. performed first-principles calculations which showed that, when used as a substrate, hexagonal boron nitride monolayer and Si-SiC preserve silicene's main electrical properties [17]. In this way these provide an interesting possibility to experiment on silicene. It is not, however, obvious if these kinds of systems could be created in practice.

2.3 From graphene to silicene

The success of graphene as the prodigy of future electronic device material has set up the way for silicene. This can be easily understood when comparing these materials. Both of the them share the same basic geometry which also leads to

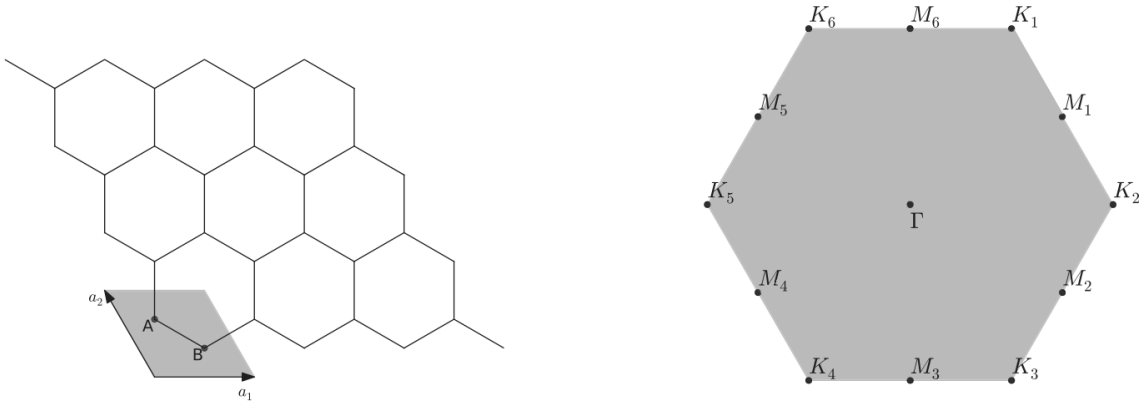

Figure 2.2: The honeycomb structure, unit cell and Brillouin zone of silicene [26].

similar electronic properties. The next two subsections will go over the geometries of these materials as well as their main electronic properties which have excited the scientific community with extraordinary qualities. Especially the differences are worth to note to understand why silicene prevails over graphene.

2.3.1 Geometry and reciprocal space

Starting from graphene, its geometry can be characterised as a honeycomb structure where each carbon atom has three nearest neighbours. The structure is fully planar and it can be decomposed into two sublattices, marked A and B in figure 2.2. Therefore the unit cell (shaded area) consists of two atoms, one from each sublattice.

Silicene shares the same honeycomb formation but includes a small buckling to the structure. Side view in figure 2.3 best demonstrates this. The sublattices have shifted so that they don't rest in the same plane anymore but rather form their own planes. Throughout this thesis the value of 0.46 ångströms is used for the buckling parameter Δ. Other sources may give slightly different values.

The buckling is the key structural aspect which separates silicene from graphene. It introduces additional properties in silicene's electronic structure. As perhaps the most important possibility, this buckling enables careful manipulation of the band gap by electric field. More of this will be presented in chapter 5.

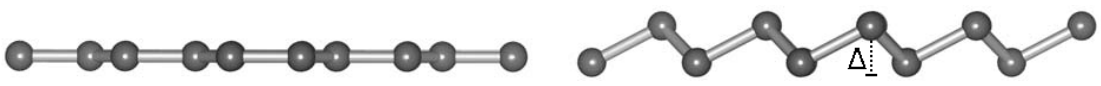

(a) Graphene (b) Silicene

Figure 2.3: Side view of (a) graphene and (b) silicene structures [13].

Turning now to the reciprocal space, it is easily seen that the Brillouin zone is hexagonal as presented in figure 2.2. This stems from the fact that the real space geometry is hexagonal as well. Important symmetry points in the Brillouin zone are

marked in the figure apart from the gamma point in the center of the zone. The corners of Brillouin zone are labeled as K or K' as these are inequivalent in the sense that they cannot be connected with a reciprocal lattice vector. The center point between neighbouring K and K' point is marked M. These high symmetry points will be used in the band structures presented later.

2.3.2 Properties

As silicene is structurally very similar to graphene, we would expect their properties to be alike. Therefore we summarize the main properties of graphene which we would expect to find in silicene as well. In fact, some of them have already been theoretically found.

Graphene has been verified to be mechanically very strong. Its breaking strength is over 100 times greater than a hypothetical steel film of the same thickness. On top of this, graphene is also more flexible than steel and very light. Its density is only 0.77 $^{mg}/_{m^2}$ and so a graphene sheet is much stronger, lighter and more flexible than a steel film.

Moreover, graphene has very high electrical conductance. This is caused by a linear dispersion relation near the K point. This is called a Dirac cone since a cone-like structure is formed in three dimensions. The Dirac cone has been shown to lead to *massless* Dirac fermions. The potential applications are obvious since electrons residing around K point could be used for very fast electronics. The minimum limit of resistivity at room temperature is as low as 10^{-6} Ωcm which is the lowest known value at this temperature regime.

Graphene also has the highest thermal conductivity of any carbon allotrope, even exceeding the thermal conductivity of diamond. For example, graphene's thermal conductivity is 10 times higher than copper's. Graphene also possesses useful optical properties as it is almost transparent. It absorbs only 2.3 % of light regardless of wavelength and therefore it has no color. [30]

A Dirac cone is also present in silicene which leads to electrical conductance comparable to graphene. However, one of graphene's big limitations is the lack of natural band gap which greatly hinders its application to electric devices. Strictly speaking this is not true because spin-orbit coupling (SOC) induces a tiny gap in graphene. This is nevertheless negligible. In silicene instead, spin-orbit interaction is much stronger leading to a small but still appreciable naturally occurring gap between valence and conduction bands. Also, the gap can be easily controlled with a perpendicular electric field giving silicene a clear advantage over graphene.

Furthermore, Xu et al. predicted giant magnetoresistance (GMR) effect in a structure consisting of zigzag silicene nanoribbon connecting two silicene sheets [36]. Besides GMR, spin-related phenomena in silicene include quantum spin Hall effect

(QSHE). This has been studied by An et al. [1], for instance. The interesting point in QSHE is that it is related to topological insulators, a new phase of matter observed not until 2007. In appropriate conditions, silicene can be characterized as a two-dimensional topological insulator whose all viable applications are not yet fully clear.

2.4 Possible applications

Since graphene has been around for some time now, a vast number of applications have been proposed. To begin with, one of the best known idea is to make field-effect transistors from graphene. The idea is provoked by the high carrier mobility due to the Dirac cone. Naturally the lack of band gap forces the use of extra tricks which complicate the manufacturing of transistors. Silicene is more viable material here for two reasons. Firstly it has larger band gap which can be easily tuned. The gap is actually still too small but Quhe et al. have shown how to overcome this difficulty by adsorption of alkali atoms [25]. Secondly silicene is more compatible with current semiconductor industry which relies heavily on silicon. In general silicene could be used in integrated circuits which would benefit from silicene's exquisite properties.

Graphene is ideal material for e.g. touchscreens, liquid crystal displays and organic photovoltaic cells which all require transparent conducting electrons. These in turn are provided by graphene's high electrical conductivity and optical transparency. The same properties also lead to an intriguing application in solar cells. Theoretically graphene solar cells could offer 60 % efficiency which is double the current maximum efficiency reached. These devices would also be very durable and flexible which is an additional advantage of graphene.

Graphene is also a prospect of distillation processes as it allows water vapor to pass through but blocks all other liquids and gases. Development of this property could be a huge improvement for biofuel or alcoholic beverage production. Furthermore, graphene is a great candidate for gas detection as its entire volume is exposed to its surroundings thanks to its two-dimensional character. As graphene is intrinsically insensitive, functionalization is required which can be accomplished by e.g. coating with suitable polymers. Adsorption of gaseous molecules on the polymer layer would then locally change the electrical resistance which is detectable thanks to graphene's high conductivity and low noise. Partly due to the same reasons graphene could also be used for mammalian and microbial detection and diagnosis.

The high thermal conductivity of graphene can be utilized if graphene is used as additive in coolants. Yu et al. reported that even as little as 5 volume percentage graphene enhances the thermal conductivity of a base fluid by 86 % [37]. Last but not least, graphene is believed to be a good material for energy storage due to its exceptionally high surface area to mass ratio. For example, ultracapacitors made

from graphene could give greater energy storage density than is currently available. As a very specific application regarding silicene, Tritsaris et al. speculated that silicene could be used as a high-capacity host of lithium in Li-ion batteries [31].

Additionally silicene contributes more as it is also a viable candidate for spintronic applications which are based on manipulating electron's spin as well as its charge. They are expected to be faster and less energy-consuming than today's traditional electronic devices. Silicene can contribute to this in more than one way. Firstly, spin filtering has been the subject in a number of publications. For instance, Tsai et al. showed how spin-polarized current can be extracted from silicene [32]. Secondly, GMR effect in silicene may be readily used as GMR as an old and well-known phenomenon has already found its way in many applications. On top of this, topological insulators have been suggested to be used in quantum computing. Thus silicene is a material to be remembered when engineering such exotic devices.

3. TIGHT-BINDING BASICS

In this thesis silicene has been studied by tight-binding (TB) method. Therefore some insight to TB model is presented in this chapter. It should be noted that even though the TB method is heavily reduced and simple picture of the physics in solids, it holds surprisingly powerful and easily implementable theory.

Tight-binding model is a semi-empirical method for modelling solids that form crystalline structures. It is based on forming the crystal wave function using atomic orbitals centered on each atom in the crystal. The term "tight binding" indicates that the crystal potential is strong. Therefore electrons are bound to atoms for a long time before moving to the next atom. In effect electrons are considered to move slowly through the lattice. TB often gives good qualitative results and can be combined with *ab initio* calculations for comparison. It can sometimes even give excellent quantitative results with a carefully adjusted parametrization.

Tight-binding method shows at least two clear perks. First and foremost, TB is computationally very light which is one of the reasons for its wide and popular usage. Secondly, different terms, for instance spin-orbit coupling, can be easily switched on or off. This allows to study individual terms and their contribution to the whole electronic structure.

3.1 Periodic crystal and Bloch sums

In the TB method our aim is to get the band structure of the material we are interested in. This means we want to know the electronic states (energies) as a function of wave vector $\mathbf{k}$. Before rushing ahead, we first need a wave function for the electron corresponding to these energies. Consequently we are using one-electron picture and begin to form the crystal wave function based on the crystal periodicity. As the simplest case it is initially assumed that the unit cell of the crystal has only one atom.

The crystal potential V is due to the atomic potentials V_{at}

$$V(\mathbf{r}) = \sum_{\mathbf{R}} V_{at}(\mathbf{r} - \mathbf{R}) \tag{3.1}$$

where the sum runs over all lattice vectors $\mathbf{R}$. We want to solve the Schrödinger equation for an electron in a periodic potential. The system is described by the

Hamiltonian

$$H = -\frac{\hbar^2}{2m}\nabla^2 + V(\mathbf{r}) \tag{3.2}$$

where $\hbar$ is the reduced Planck's constant and m is electron mass.

In a periodic crystal it is reasonable to assume that the crystal wave function is related to the orbitals of the atoms that constitute the crystal. Again, it is intuitive that the wave function should show the same periodicity as the underlying lattice. This is where Bloch's theorem steps in. We want to form a periodic wave function and an appropriate guess is

$$B_{n,\mathbf{k}}(\mathbf{r}) = \frac{1}{\sqrt{N}} \sum_{\mathbf{R}} \mathrm{e}^{\mathrm{i}\mathbf{k}\cdot\mathbf{R}} \phi_n(\mathbf{r} - \mathbf{R}). \tag{3.3}$$

This is called a "Bloch sum" and it is formed from the atomic orbitals ϕ_n accompanied with a phase factor since the orbitals are located on different sites. Here n tells which orbital is in question – s, p, d etc. – and N is the number of unit cells in the whole crystal. It is straightforward to see that the Bloch sum in equation 3.3 satisfies the Bloch condition

$$B_{n,\mathbf{k}}(\mathbf{r} + \mathbf{R}_0) = \mathrm{e}^{\mathrm{i}\mathbf{k}\cdot\mathbf{R}_0} B_{n,\mathbf{k}}(\mathbf{r}) \tag{3.4}$$

and is therefore a valid guess for the wave function we are looking for.

3.2 Basis functions

Now we have a wave function for an electron in the crystal. However, the wave function postulated so far is formed of only one type of atomic orbital. In general we want the crystal wave function to be a mixture of different atomic orbitals because often atoms have multiple types of orbitals in the valence shell. It follows that the final wave function Ψ we are looking for is a linear combination of Bloch sums

$$\Psi_{\mathbf{k}}(\mathbf{r}) = \sum_n c_n(\mathbf{k}) B_{n,\mathbf{k}}(\mathbf{r}). \tag{3.5}$$

This allows Ψ to have mixture of atomic orbital characters. In effect we have now defined the Bloch sums to be the basis functions of the crystal wave function. Each of the Bloch sums, or rather each of the atomic orbitals, included in the TB model leads to its own energy band. Since the interesting things are due to the valence electrons, only valence orbitals are usually included in any realistic model. Sometimes one can use unoccupied orbitals as well to get a better description of conduction bands.

Having formed a wave function we are happy with, it remains to solve the Schrödinger equation

$$H\Psi_{\mathbf{k}} = \epsilon_{\mathbf{k}}\Psi_{\mathbf{k}} \tag{3.6}$$

where it is explicitly indicated that the energies ϵ are a function of the wave vector. Solving the equation is best done in matrix form. Getting there will be the subject of the next section.

3.3 Matrix formulation

Quantum mechanically the Hamiltonian matrix elements $H_{m,n}$ are integrals between basis functions with respect to the Hamiltonian. To get them we simply need to multiply the Schrödinger equation in 3.6 on the left by the complex conjugate of another Bloch sum $B_{m,\mathbf{k}}$. After this we integrate over the whole crystal.

After multiplication and integration the left hand side of equation 3.6 is

$$\langle B_{m,\mathbf{k}} \,|\, H \,|\, \Psi_{\mathbf{k}} \rangle \equiv \sum_n c_n(\mathbf{k}) \int B^*_{m,\mathbf{k}}(\mathbf{r}) H B_{n,\mathbf{k}}(\mathbf{r}) = \sum_n H_{m,n}(\mathbf{k}) c_n(\mathbf{k}). \tag{3.7}$$

What we have achieved here is to extract the matrix elements between two basis functions, one formed from n-type atomic orbitals, the other from m-type orbitals. Similarly the right hand side has the form

$$\langle B_{m,\mathbf{k}} \,|\, \epsilon_{\mathbf{k}} \,|\, \Psi_{\mathbf{k}} \rangle \equiv \epsilon_{\mathbf{k}} \sum_n c_n(\mathbf{k}) \int B^*_{m,\mathbf{k}}(\mathbf{r}) B_{n,\mathbf{k}}(\mathbf{r}) = \epsilon_{\mathbf{k}} \sum_n S_{m,n}(\mathbf{k}) c_n(\mathbf{k}). \tag{3.8}$$

The matrix S directly measures the extent of overlap between functions $B_{m,\mathbf{k}}$ and $B_{n,\mathbf{k}}$. As the Bloch sums are formed from atomic orbitals, the matrix S actually tells the overlap between atomic orbitals. Therefore it is called the overlap matrix.

Whether it is obvious or not, we have formulated a matrix equation with Bloch sums as the basis functions. Writing equations 3.7 and 3.8 implicitly, we have a generalized eigenvalue problem

$$H(\mathbf{k})\mathbf{c}(\mathbf{k}) = \epsilon_{\mathbf{k}} S(\mathbf{k})\mathbf{c}(\mathbf{k}). \tag{3.9}$$

At this point there is only one problem left. We need to know what the matrix elements are. As it turns out, this is fairly easily solved. This is also where the empirical part of tight-binding turns up.

3.4 Hopping integrals

We are looking for the Hamiltonian matrix elements $H_{m,n}(\mathbf{k})$ as defined in equation 3.7 by the Bloch sums. The natural way to follow is to insert the Bloch sum definitions (equation 3.3) into this and see what will happen. If we change the

summation indexes in the Bloch sum definitions from $\mathbf{R}$ to $\mathbf{R_1}$ and $\mathbf{R_2}$, we get

$$\begin{aligned} H_{m,n}(\mathbf{k}) &= \frac{1}{N} \sum_{\mathbf{R_1},\mathbf{R_2}} \mathrm{e}^{\mathrm{i}\mathbf{k}\cdot(\mathbf{R_2}-\mathbf{R_1})} \int \phi_m^*(\mathbf{r}-\mathbf{R_1}) H \phi_n(\mathbf{r}-\mathbf{R_2}) \\ &= \frac{1}{N} \sum_{\mathbf{R_1},\mathbf{R_2}} \mathrm{e}^{\mathrm{i}\mathbf{k}\cdot(\mathbf{R_2}-\mathbf{R_1})} H_{m,n}(\mathbf{R_2}-\mathbf{R_1}) \end{aligned} \tag{3.10}$$

From this we see that the matrix element depends only on the difference $\mathbf{R_2} - \mathbf{R_1}$ and not $\mathbf{R_1}$ or $\mathbf{R_2}$ individually. We can then simply sum over one index, $\mathbf{R}$, which still goes through the whole crystal. The other sum in 3.10 then just gives the number of unit cells N in the crystal. In summary, the Hamiltonian matrix elements are of the form

$$H_{m,n}(\mathbf{k}) = \sum_{\mathbf{R}} \mathrm{e}^{\mathrm{i}\mathbf{k}\cdot\mathbf{R}} H_{m,n}(\mathbf{R}) \tag{3.11}$$

where we have defined

$$H_{m,n}(\mathbf{R}) = \int \phi_m^*(\mathbf{r}) H \phi_n(\mathbf{r}-\mathbf{R}). \tag{3.12}$$

The elements $H_{m,n}(\mathbf{R})$ are between atomic orbitals ϕ_m centered at the origin and ϕ_n centered at $\mathbf{R}$. The integral 3.12 therefore measures the amplitude that an electron in orbital ϕ_n moves, or *hops*, to the orbital ϕ_m. Since the basic assumption of TB model was to assume strong ionic potential, this amplitude cannot be too large. Also, when $|\mathbf{R}|$ is large the orbitals ϕ_n and ϕ_m do not overlap appreciably and the integral is negligible. This allows us to confine ourselves to a few nearest neighbours at most.

However this still doesn't tell us what the actual value of the matrix element $H_{m,n}(\mathbf{k})$ is. In fact, the TB model doesn't explicitly tell us this. The values $H_{m,n}(\mathbf{R})$ are rather taken as constant parameters to TB model and are called *hopping parameters*. In practice the hopping parameters can be found out by fitting to *ab initio* calculations, for example. It is also worth noting that they depend on the distance $|\mathbf{R}|$. Thus we need a hopping parameter for every value of $|\mathbf{R}|$. Luckily we only need to consider nearest neighbours as discussed above.

One special case is $H_{m,n}(\mathbf{0})$ where we now have a matrix element between orbitals n and m centered on the same site. To study this, it is useful to split the crystal potential V in equation 3.1 into two parts

$$V(\mathbf{r}) = V_{at}(\mathbf{r}) + V'(\mathbf{r}) \tag{3.13}$$

where the first term is the potential due to the atom at the origin and the second term contains the potential due to all the other atoms. This means $V'(\mathbf{r})$ is small

near the origin and we can write

$$\begin{aligned} H_{m,n}(\mathbf{0}) &= \langle \phi_m(\mathbf{r}) \,|\, H \,|\, \phi_n(\mathbf{r}) \rangle \\ &= \left\langle \phi_m(\mathbf{r}) \,\middle|\, \left(-\frac{\hbar^2}{2m}\nabla^2 + V_{at}(\mathbf{r}) \right) \,\middle|\, \phi_n(\mathbf{r}) \right\rangle + \langle \phi_m(\mathbf{r}) \,|\, V'(\mathbf{r}) \,|\, \phi_n(\mathbf{r}) \rangle \,. \end{aligned} \tag{3.14}$$

The first term involves two atomic orbitals on the same site with the Hamiltonian being the atomic Hamiltonian. Therefore the first term equals to the atomic eigenvalue ε_n if the orbitals are the same. Otherwise the result is zero since atomic orbitals are orthogonal to each other. The second term instead can be neglected because it involves two orbitals at the origin together with a potential that is small there. To summarize, the term $H_{m,n}(\mathbf{0})$ can be approximated as

$$H_{m,n}(\mathbf{0}) = \varepsilon_n \delta_{mn} \tag{3.15}$$

where δ_{mn} is the Kronecker delta. These are called *on-site* energies. [21].

One useful point should be remembered here. We don't actually need to use the atomic orbital energies as our on-site terms since we can define the energy reference point arbitrarily. Hence it is common to set the on-site terms to zero. When we are using different orbitals, however, their relative difference should be maintained.

Lastly, there is the notational part of hopping integrals. The common notation used in tight binding models is followed in the subsequent chapters. Therefore it is time to introduce the parameter t which is just the hopping integral defined in equation 3.12

$$t_{m,n}(\mathbf{R}) \equiv H_{m,n}(\mathbf{R}). \tag{3.16}$$

In effect, TB models present a hopping parameter for every pair of orbitals m and n and for every distance $|\mathbf{R}|$ that includes a new neighbour.

Furthermore, often second quantized notation is used when presenting tight-binding models. In this formalism the Hamiltonian including only one hopping parameter is presented as

$$H = -t \sum_{\langle i,j \rangle, \sigma} c^\dagger_{i\sigma} c_{j,\sigma} \tag{3.17}$$

where $c^\dagger$ is the creation operator, c annihilation operator and the sum runs over all nearest-neighbours $\langle i, j \rangle$ and spin states (up or down) σ. The phase factors $\mathrm{e}^{\mathbf{ik}\cdot\mathbf{R}}$ which entail the wanted $\mathbf{k}$-dependence get hidden in this representation as they are not written explicitly anymore.

The Hamiltonian in equation 3.17 includes electron's spin which is unnecessary for the bare hopping term. Hopping from one orbital to another does not change spin state and has the same magnitude for both spin states. However, in future models we will include terms which depend on spin. Hence the spin polarization

has been included to the bare hopping Hamiltonian. In practice it means that the hopping Hamiltonian is a block diagonal matrix where both blocks correspond to different spin. Also, since the blocks are identical, the system is spin-degenerate.

3.5 Generalization to multi-atom unit cell

So far the discussion has been limited to a simple unit cell containing only one atom. Despite this, the results do not change when multiple atoms in the unit cell are allowed. To be sure of this, the following briefly presents the generalization of the previous results.

The generalization is easy to implement and doesn't entail additional difficulties. However, the notation is starting to get somewhat awkward. As it cannot be avoided, let's include additional subscript i which specifies the particular atom in the unit cell we are dealing with. The atomic orbitals which the Bloch sums are formed of are now $\phi_{n,i}(\mathbf{r}-\mathbf{R}-\tau_i)$ where τ_i indicates the position of the i-th atom with respect to the origin of the cell at $\mathbf{R}$. Using these the Bloch sums in equation 3.3 generalize to

$$B_{n,i,\mathbf{k}}(\mathbf{r}) = \frac{1}{\sqrt{N}} \sum_{\mathbf{R}} \mathrm{e}^{\mathrm{i}\mathbf{k}\cdot(\mathbf{R}+\tau_i)} \phi_n(\mathbf{r}-\mathbf{R}-\tau_i). \tag{3.18}$$

The crystal wave function is still defined according to equation 3.5 with the addition that the sum now extends over i as well since we want to take all atoms into account. It should also be remembered that the atoms in unit cell can be different (in this case we have a compound) and we could include different orbitals from different types of atoms in the basis. As such the coefficients c depend on i as well.

Going back to determining the Hamiltonian matrix elements in equation 3.10, we now get

$$\begin{aligned} H_{m,i;n,j}(\mathbf{k}) &= \frac{1}{N} \sum_{\mathbf{R_1},\mathbf{R_2}} \mathrm{e}^{\mathrm{i}\mathbf{k}\cdot(\mathbf{R_2}+\tau_j-\mathbf{R_1}-\tau_i)} \int \phi_m^*(\mathbf{r}-\mathbf{R_1}-\tau_i) H \phi_n(\mathbf{r}-\mathbf{R_2}-\tau_j) \\ &= \mathrm{e}^{-\mathrm{i}\mathbf{k}\cdot\tau_i} \left(\sum_{\mathbf{R}} H_{m,i;n,j}(\mathbf{R}+\tau_j-\tau_i) \mathrm{e}^{\mathrm{i}\mathbf{k}\cdot\mathbf{R}} \right) \mathrm{e}^{\mathrm{i}\mathbf{k}\cdot\tau_j}. \end{aligned} \tag{3.19}$$

This look exactly like equation 3.11 apart from the two additional phase factors on both sides. As a matter of fact, the phase factors are superfluous as they can be regarded as a unitary transformation acting on the matrix in parenthesis. Since the matrix involved is Hermitian, its eigenvalues do not change under unitary transformation and the additional phase factors can be disregarded. As a result we regain the same basic result as in the simple one-atom case.

As was claimed, multi-atom unit cell isn't basically any different from the initial assumption that the unit cell contains only one atom. Only additional notation

has been introduced. Furthermore, nothing has been said about the overlap matrix S thus far. This is because in this thesis it is totally omitted by setting it to identity matrix. This can done because the overlap matrix is defined analogously to equation 3.11

$$S_{m,n}(\mathbf{k}) = \sum_{\mathbf{R}} \mathrm{e}^{\mathrm{i}\mathbf{k}\cdot\mathbf{R}} S_{m,n}(\mathbf{R}) \tag{3.20}$$

where $S_{m,n}(\mathbf{R})$ denotes the integral $\int \phi_m^*(\mathbf{r})\phi_n(\mathbf{r}-\mathbf{R})$. Now it it assumed that the atomic orbitals are normalized and do not overlap at all. That is, whenever $\mathbf{R} \neq \mathbf{0}$ holds, the integral goes to zero. Only when m equals n and the orbitals are at the same site the integral will be nonzero, namely one.

3.6 Two-center approximation and angular dependency

There are further difficulties related to the hopping integrals we have not yet considered. The definition of hopping integral in equation 3.12 is composed of three parts: two atomic orbitals and the Hamiltonian. Since we defined the crystal potential according to equation 3.1, the integral consists of many terms which in general have contributions from three regions. These regions are located around the orbitals ϕ_n and ϕ_m as well as around the atomic potential V_{at}. Depending on where the regions are located at we have four different cases:

1. If the orbitals and the atomic potential all lie on the same site, we have the on-site integral introduced in section 3.4.

2. If the orbitals lie on separate sites with the potential locating at the same site with one of the orbitals, we have a two-center integral.

3. If all regions are located at different sites, we have a three-center integral.

4. The final situation arises when both orbitals are on the same site with the potential being somewhere else.

The last case, number four, was originally neglected by Slater and Koster when they introduced their tight-binding method in 1954. It can be considered as a correction to the on-site energies according to equation 3.14 but is omitted here as already stated. [23].

Furthermore, the *two-center approximation* is now introduced to be used in this thesis. It simply means that we ignore the three-center integrals so that the potential is always located at the site of one or the other orbital. Therefore the hopping parameters depend only on the relative position between the orbital sites like was assumed and stated earlier. It should be emphasized that the two-center approximation is not always valid but usually leads to a good description of the electronic structure.

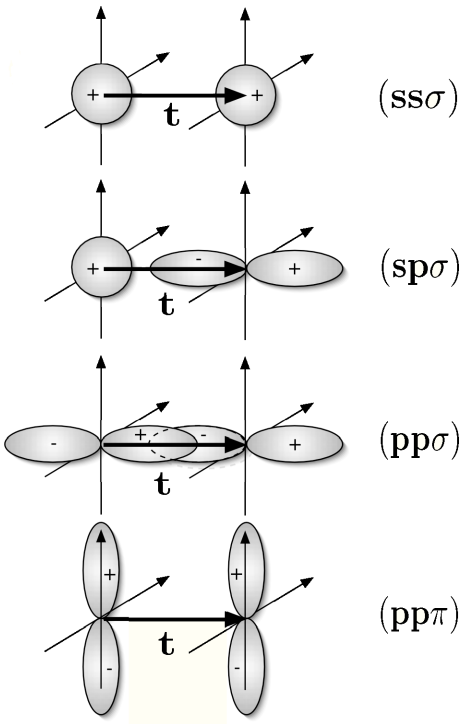

Figure 3.1: The fundamental hopping integrals of s and p orbitals.

The last issue in understanding the nature of hopping integrals is their angular variation. This hasn't got any consequence in the case of hopping between two s orbitals since they are spherically symmetric and look the same when viewed from any direction. However, when p orbitals are introduced we can have π-bonds as well as σ-bonds between two orbitals as illustrated in figure 3.1. The fundamental hopping integrals are labeled as (ssσ), (spσ), (ppσ) and (ppπ) indicating the orbitals involved and the nature of the bond. The signs of these basic parameters can be readily deduced. Since two s orbitals have the same sign, the integral (ssσ) must be negative. Correspondingly, the element (spσ) must be positive since it involves overlap of lobes of opposite sign. It then follows that the integral (ppσ) is positive and (ppπ) is negative.

If we take two p orbitals forming a σ-bond (look at the integral (ppσ) in figure 3.1) and start to rotate the other orbital around the other, the hopping integral changes. When the angle is zero degrees the integral is purely σ-type and once the angle reaches 90 degrees, we have a pure π bond. In between the integral is a mixture of π and σ-types with the actual amounts depending on the angle of rotation. Similarly there is angular variation in the hopping integral between s and p orbital. These have been tabulated up to d orbitals by Slater and Koster [27]. Here we only need the integrals between s and p and two p atomic states which can be found in table 3.1. Here l, m and n are the direction cosines of the vector from the left state to the right state with direction cosine meaning the cosine of the angle between a vector and

Table 3.1: Slater-Koster table for angular dependencies of hopping integrals.

$t_{\mathrm{s,s}}$	$(\mathrm{ss}\sigma)$
$t_{\mathrm{s,x}}$	$l(\mathrm{sp}\sigma)$
$t_{\mathrm{x,x}}$	$l^2(\mathrm{pp}\sigma) + (1-l^2)(\mathrm{pp}\pi)$
$t_{\mathrm{x,y}}$	$lm(\mathrm{pp}\sigma) - lm(\mathrm{pp}\pi)$
$t_{\mathrm{x,z}}$	$ln(\mathrm{pp}\sigma) - ln(\mathrm{pp}\pi)$

a coordinate axis. That is, the direction cosine l is with respect to x-axis, m with respect to y-axis and n with respect to z-axis. The subscripts x, y and z refer to the three p orbitals. The missing hopping integrals can be constructed by permutation of indices and cosine directions. [28].

In addition, certain symmetric situations make hopping integrals vanish. For instance, considering $\mathrm{p_x}$ and $\mathrm{p_y}$ orbitals both lying in x-axis, the resulting hopping integral is zero because contributions from different lobes cancel each other. This can be routinely seen from table 3.1 as well where the value of m in this case would be zero.

4. GREEN'S FUNCTION THEORY

Green's functions are a powerful tool which together with TB method provides versatile arsenal to study solids. Their usefulness stems from the fact that most properties of the system are related to them. In particular transport properties are systematically calculated from Green's functions. Here however we don't need to delve so deep into the formalism.

This chapter covers the topic of Green's functions to the extent that is relevant and utilized in the following chapters. This includes the basic connection of Green's function to density of states with emphasis to its local distribution. All in all Green's function formalism is but a small part of the thesis. Nevertheless, it has an important role. With Green's functions we are able to study silicene in real space through localized DOS. In addition we will be focusing on spins separately to find out if a system exhibits spin-dependent features.

4.1 Basics of Green's function

Green's function $G(E)$ is defined through the Hamiltonian as

$$(E - H)G(E) = I \tag{4.1}$$

where E is energy and I the identity matrix. From the above equation it is easy to see that we could calculate the Green's function of the system by simply inverting the operator $E - H$. It can therefore be regarded as an operator in the same way that the Hamiltonian is with the exception that it is also a function of energy. [38].

To proceed, Green's function in time space acts as a propagator of a particle from time t to a later time t'. It is thus natural to expect that the Green's function is causal meaning that the future events do not affect the present. In practice we mean to say that the time dependent Green's function $G(t, t')$ is zero whenever the condition $t > t'$ holds. We can get the energy dependent Green's function $G(E)$ from $G(t, t')$ through Fourier transformation where the causality restriction is implemented by a vanishing imaginary part $\mathrm{i}\eta$. This is generally called a retarded Green's function $G^+(E)$ but here we drop both the pre-qualifier and the superscript and define the Green's function as

$$G(\mathbf{k}, E) = (E - H + \mathrm{i}\eta)^{-1} \equiv ((E + \mathrm{i}\eta)I - H)^{-1} \tag{4.2}$$

where the last equivalence wishes to clearly indicate that we are dealing with matrices and shows the appropriate form for the Green's function matrix. The **k**-dependence has also been explicitly indicated since the tight-binding Hamiltonian depends on it. [22].

Now, splitting the Green's function into a sum running over all the eigenstates ψ_n of the Hamiltonian, the following is equivalent to equation 4.2:

$$G(\mathbf{k}, E) = \sum_n \frac{\psi_n(\mathbf{r})\psi_n^*(\mathbf{r})}{E - \epsilon_n + \mathrm{i}\eta} = \sum_n |n\rangle \frac{1}{E - \epsilon_n + \mathrm{i}\eta} \langle n| \,. \tag{4.3}$$

In this basis the Green's function matrix is diagonal. It is also clear that the eigenvalues of the Green's function operator are just the inverse of the operator $E - H + \mathrm{i}\eta$. Green's function peaks sharply near the Hamiltonian eigenvalues ϵ_n and thereby gives the electronic spectrum. Generalizing equation 4.3, the Green's function can be expressed in any basis. Particularly, we want to use the TB basis from which we take the states a and b to obtain a non-diagonal matrix representation

$$G_{ab}(\mathbf{k}, E) = \sum_n \frac{\langle a \,|\, n\rangle \langle n \,|\, b\rangle}{E - \epsilon_n + \mathrm{i}\eta} = \sum_n \frac{c_a(n)c_b^*(n)}{E - \epsilon_n + \mathrm{i}\eta}. \tag{4.4}$$

The linear combination coefficients $c_a(n)$ and $c_b(n)$ describe how strongly the states a and b contribute to the eigenstates. To study individual orbitals and their contribution to the energy bands we can calculate the Green's function partially by setting both states in equation 4.4 to be the same, i.e. we look at the diagonal elements. Therefore the numerator $c_a(n)c_b^*(n)$ becomes $|c_a(n)|^2$ which is just the norm squared of the corresponding linear combination coefficient. To get the total contribution from all the orbitals in our basis, we only need to sum over all of them. Interestingly we can also choose to look at the cross terms between orbitals which comes with an additional feature: the complex phase leading to interference effects. Here however we are only interested in the diagonal terms. [20].

To close the discussion of defining the Green's function, the precise connection to the tight-binding models is now established. In fact, we want to differentiate between the two spin states and recalling that the TB basis consists of atomic orbitals centered on different sites, we write the equation 4.4 again as

$$G_{i\sigma,j\sigma'}(\mathbf{k}, E) = \sum_n \frac{c_{i\sigma}(n)c_{j\sigma'}^*(n)}{E - \epsilon_n + \mathrm{i}\eta}. \tag{4.5}$$

Here i and j mark the atomic orbitals and σ labels the spin state. The coefficients give the spectral weight of each orbital and are obtained by solving equation 3.9.

4.2 Density of states

There is a very fundamental connection between Green's function and density of states (DOS). The density of states ρ of the system is given by the imaginary part of the Green's function $\Im[G]$ as [38]

$$\rho(\mathbf{k}, E) = -\frac{1}{\pi}\Im[G(\mathbf{k}, E)]. \tag{4.6}$$

At this point it is fair to wonder what the role of the imaginary part $i\eta$ of the Green's function is. In fact, in the case of DOS it can be seen to be connected to the width of the energy levels. In effect, the larger η is, the broader are the energy levels. We can use this to our advantage by using an appropriate value for η according to the level of needed resolution.

We are also interested in the local density of states (LDOS). According to equation 4.5 we obtain LDOS which is even partitioned to spin densities of states:

$$\rho_{i\sigma}(\mathbf{k}, E) = -\frac{1}{\pi}\Im[G_{ii\sigma}(\mathbf{k}, E)]. \tag{4.7}$$

This tells the DOS at the site i of the system. In addition, we can choose to look at the different spins individually. All in all this is a very useful equation in the sense that it makes it possible to study localized effects. For example the density of states is very different at the edge compared to the bulk deeper in the sample.

We will mainly be using equation 4.7 to calculate LDOS projections on a $\mathbf{k}$-E grid to see how the bands are distributed in real space and if they are spin polarized. In effect basic TB calculations gives us the overall band structure. Through Green's function formalism we can then study where individual bands come from.

5. MODELLING OF BULK SILICENE

Ab initio calculations stand physically on solid ground and they would give the most precise results. Despite this we can study silicene with the simplified picture given by TB models which are accurate enough for our purposes. In addition to being very light, TB calculations offer the possibility of studying different interactions and terms individually. We will be taking full advantage of this as well.

We now apply tight-binding theory to silicene. To be more precise, we start with a fully periodic system, i.e. bulk silicene, in which we use nearest-neighbour TB model. This means that we can restrict ourselves to only one hopping parameter per distinct pair of neighbouring orbitals. Recall also that every atom in silicene structure has three nearest neighbours (figure 2.2).

In addition, here we go further than the bare hopping model takes us by studying the effect of spin-orbit coupling on the electronic structure. Together with an electric field, SOC induces interesting physical phenomena which will be revealed in the following discussion.

5.1 Band structure

Silicon has the electron configuration of $[\mathrm{Ne}]3s^2 3p^2$ indicating that both s and p orbitals are occupied in the valence shell. Therefore we form the TB basis from s, p_x, p_y and p_z orbitals. In fact, s and the two p orbitals, p_x and p_y, lying on the same plane as the silicene sheet, are responsible for holding the structure together. On the contrary, p_z orbital points perpendicular to the silicene sheet and is responsible for the interesting electronic properties. The Hamiltonian derived here is based on the model by Vogl et al. [33] who used it to study semiconductors such as silicon. Here we apply the same parametrization to silicene. This controversy leads to a rather faulty band structure but most importantly it is qualitatively right.

Silicene has two atoms in the unit cell of the lattice as showed in figure 2.2. This implies an 8×8 Hamiltonian since we have two atoms each holding 4 orbitals. The task is to form the Hamiltonian in equation 3.11 in the basis of $\{s_1, p_{x1}, p_{y1}, p_{z1}, s_2, p_{x2}, p_{y2}, p_{z2}\}$. It is easily seen that the Hamiltonian can be divided to blocks

$$H = \begin{bmatrix} A & B \\ B' & A \end{bmatrix} \tag{5.1}$$

where A and B are 4×4 matrices. The block A holds only the on-site terms, equation 3.15, and it is diagonal

$$A = \begin{bmatrix} E_s & 0 & 0 & 0 \\ 0 & E_p & 0 & 0 \\ 0 & 0 & E_p & 0 \\ 0 & 0 & 0 & E_p \end{bmatrix}. \tag{5.2}$$

Here E_s and E_p are the energies of the s and p orbitals.

The block B holds the inter-atomic terms, i.e. the hopping terms, which signify the electron movement in the crystal. In short, B is basically the following matrix

$$\tilde{B} = \begin{bmatrix} t_{\mathrm{s,s}} & t_{\mathrm{s,x}} & t_{\mathrm{s,y}} & t_{\mathrm{s,z}} \\ t_{\mathrm{x,s}} & t_{\mathrm{x,x}} & t_{\mathrm{x,y}} & t_{\mathrm{x,z}} \\ t_{\mathrm{y,s}} & t_{\mathrm{y,x}} & t_{\mathrm{y,y}} & t_{\mathrm{y,z}} \\ t_{\mathrm{z,s}} & t_{\mathrm{z,x}} & t_{\mathrm{z,y}} & t_{\mathrm{z,z}} \end{bmatrix} \tag{5.3}$$

after we have multiplied each element with the corresponding phase factor $\mathrm{e}^{\mathbf{i}\mathbf{k}\cdot\mathbf{R}}$ and summed over the three neighbours. That is, the first element, for example, is calculated from $B(1,1) = \sum_{j=1}^{3} \mathrm{e}^{\mathbf{i}\mathbf{k}\cdot\mathbf{R}_j} t_{\mathrm{s,s}}$. The vectors $\mathbf{R}_j$ connecting an atom to its neighbours are easily deduced by noting that the three neighbouring atoms are at the corners of an equilateral triangle around the center atom. It follows that the angle between vectors $\mathbf{R}_i$ and $\mathbf{R}_{j\neq i}$ is 120 degrees. The lattice constant a of silicene is 3.86 ångströms giving a distance of about 2.28 ångströms between nearest neighbours. Consequently this is also the length of each vector $\mathbf{R}_j$. Note that neighbouring atoms belong to different sublattices, i.e. they are not in the same plane (buckling parameter $\Delta = 0.46$ Å). The full set of parameters used in the calculation is given in table 5.1. It should be noted that the value of (ppπ) is -0.72 eV whereas usually -1.6 eV is used. Despite this we stick with the value given in the table throughout this whole work.

Table 5.1: Tight-binding parameters used in the calculation of the band structure. From Vogl et al. [33].

Parameter	**Value (eV)**
E_s	-4.2
E_p	1.715
(ssσ)	-2.08
(spσ)	2.48
(ppσ)	2.72
(ppπ)	-0.72

Lastly we can take advantage of a trick which allows us to save some computational time and trouble. Since the Hamiltonian must be Hermitian, we only need to calculate the matrix elements above the main diagonal. The elements below the diagonal are then straightforwardly obtained from the complex conjugates of the calculated elements. This was already marked in equation 5.1 where B' indicates the complex conjugate transpose of matrix B.

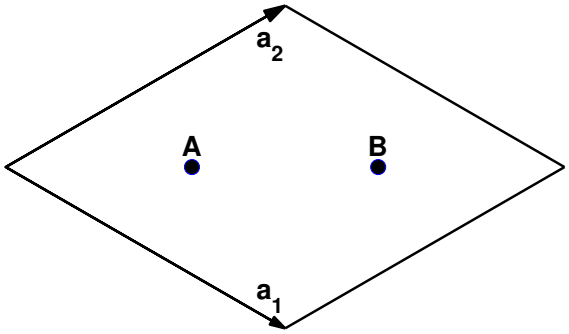

Figure 5.1: Unit cell and lattice vectors.

There remains the issue of choosing the path in reciprocal space along which the band structure will be plotted. At first, however, lattice vectors and reciprocal lattice vectors should be defined. The computational unit cell along with the lattice vectors are shown in figure 5.1 where the lattice vectors are

$$\mathbf{a}_1 = \frac{a}{2}\begin{pmatrix}\sqrt{3} & -1 & 0\end{pmatrix} \tag{5.4}$$

$$\mathbf{a}_2 = \frac{a}{2}\begin{pmatrix}\sqrt{3} & 1 & 0\end{pmatrix}. \tag{5.5}$$

The atoms belong to different sublattices with A lying higher and B lower. The corresponding reciprocal lattice vectors are

$$\mathbf{b}_1 = 2\pi\frac{\mathbf{a}_2 \times \mathbf{a}_3}{\mathbf{a}_1 \cdot \mathbf{a}_2 \times \mathbf{a}_3} = \frac{2\pi}{a}\begin{pmatrix}\frac{1}{\sqrt{3}} & -1 & 0\end{pmatrix} \tag{5.6}$$

$$\mathbf{b}_2 = 2\pi\frac{\mathbf{a}_3 \times \mathbf{a}_1}{\mathbf{a}_2 \cdot \mathbf{a}_3 \times \mathbf{a}_1} = \frac{2\pi}{a}\begin{pmatrix}\frac{1}{\sqrt{3}} & 1 & 0\end{pmatrix} \tag{5.7}$$

where the last lattice vector $\mathbf{a}_3$ simply points to the z-direction.

Next we choose to plot the band structure along the path Γ–K–M–Γ. The symmetry points are shown in figure 2.2 with the specific coordinates being

$$\mathrm{K} = \frac{1}{3}\mathbf{b}_1 + \frac{2}{3}\mathbf{b}_2 \tag{5.8}$$

$$\mathrm{M} = \frac{1}{2}\mathbf{b}_2. \tag{5.9}$$

The calculated band structure is shown in figure 5.2. Most notably there is a linear

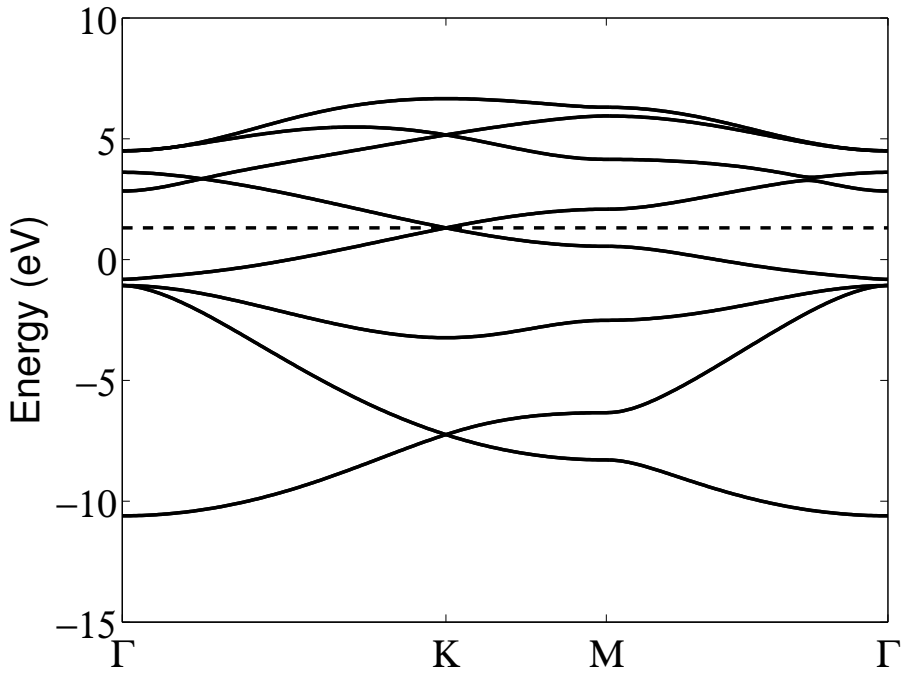

Figure 5.2: Band structure of silicene. Dashed line marks the Fermi-energy.

dispersion of the bands near the K point at the energy of approximately 1.3 electron volts. The point where the bands cross is called Dirac point. Recall that the effective mass of a particle depends on the band curvature through the relation

$$m^* = \hbar^2 \left(\frac{d^2 E}{dk^2} \right)^{-1}. \tag{5.10}$$

Hence it can be immediately seen that the effective mass is very small at Dirac point due to large curvature. This in turn leads to very high carrier mobility. Since the Fermi-energy also rests at the Dirac point, we can conclude that it is the most important feature of silicene band structure as conduction electrons are located near K point in low temperatures. Note also for future reference that there is no band gap as the bands cross each other at K point.

Another thing to point out is that the band structure in figure 5.2 doesn't faithfully mimic *ab initio* results. This is mainly due to the less-than-perfect parametrization. However, the important features are produced and basically the only task to be done is to tune the bands up or down in the energy scale.

5.2 Spin-orbit interaction

Spin-orbit coupling is a relativistic effect which couples particle's spin with its motion. In atoms it splits degenerate states leading to a fine structure of the atomic levels. The same kind of treatment leads to splitting of the bands in solids as well.

However, the real significance of SOC comes in the form of inter-atomic coupling which is **k**-dependent.

We begin with a somewhat simpler case and first look at the spin-orbit interaction within an atom as described by Petersen and Hedegård [24]. We add their model to the Hamiltonian used so far. This is followed by the spin-orbit interaction between next nearest neighbours at which point we will change to a one-band Hamiltonian. The inter-atomic spin-orbit interaction turns out to have a clear significance in silicene.

5.2.1 L · S coupling

Think of an electron orbiting the nucleus. As charged particles the protons create an electric field around the atom. The electron feels it and experiences a magnetic field

$$\mathbf{B} = -\frac{\mathbf{v} \times \mathbf{E}}{c^2} = \frac{\mathbf{v} \times \nabla V}{c^2} \tag{5.11}$$

where $\mathbf{v}$ is electron's velocity, $\mathbf{E}$ electric field, c speed of light and V potential. The electric field produced by the nucleus is spherically symmetric. Thus it depends only on the distance r from the nucleus and we can write

$$\nabla V = \frac{\mathbf{r}}{r}\frac{\mathrm{d}V}{\mathrm{d}r}. \tag{5.12}$$

Note that this is the same treatment that is used in determining spin-orbit interaction in single atoms. In solids, however, and particularly in silicene there isn't spherical symmetry. Therefore this is only an approximation. In any case, electron's spin couples to the magnetic field leading to interaction

$$U_{so} = \frac{e}{2m}\mathbf{S} \cdot \mathbf{B} \tag{5.13}$$

where m is electron mass, e its charge and $\mathbf{S}$ is the spin operator. The additional divisor 2 comes from the Thomas precession correction.

When equation 5.12 is substituted into equation 5.11, a little arithmetics gives us the following form for the interaction [9]

$$\begin{aligned} U_{so} &= \frac{e}{2mc^2}\mathbf{S} \cdot \mathbf{v} \times \mathbf{r}\frac{1}{r}\frac{\mathrm{d}V}{\mathrm{d}r} \\ &= \frac{e}{2m^2c^2}\mathbf{S} \cdot \mathbf{p} \times \mathbf{r}\frac{1}{r}\frac{\mathrm{d}V}{\mathrm{d}r} \\ &= -\frac{e}{2m^2c^2}\frac{1}{r}\frac{\mathrm{d}V}{\mathrm{d}r}\mathbf{L} \cdot \mathbf{S} \\ &= \lambda \mathbf{L} \cdot \mathbf{S}. \end{aligned} \tag{5.14}$$

In the last line we have put every constant in front of the operator $\mathbf{L} \cdot \mathbf{S}$ into a

single constant λ which we will once again take as a TB parameter. It measures the strength of the spin-orbit coupling.

Let's take now a deeper look into the spin-orbit interaction operator. First, the components of the spin operator can be expressed in terms of the Pauli matrices

$$S_x = \frac{\hbar}{2}\begin{bmatrix} 0 & 1 \\ 1 & 0 \end{bmatrix} \qquad S_y = \frac{\hbar}{2}\begin{bmatrix} 0 & -\mathrm{i} \\ \mathrm{i} & 0 \end{bmatrix} \qquad S_z = \frac{\hbar}{2}\begin{bmatrix} 1 & 0 \\ 0 & -1 \end{bmatrix}. \tag{5.15}$$

Writing out the dot product gives

$$\begin{aligned} \mathbf{L}\cdot\mathbf{S} &= L_xS_x + L_yS_y + L_zS_z \\ &= \frac{\hbar}{2}\begin{bmatrix} L_z & L_x - \mathrm{i}L_y \\ L_x + \mathrm{i}L_y & -L_z \end{bmatrix} \\ &= \frac{\hbar}{2}\begin{bmatrix} L_z & L_- \\ L_+ & -L_z \end{bmatrix} \end{aligned} \tag{5.16}$$

where L_+ and L_- are the raising and lowering operators, respectively. The operator is now in a useful form since we now just need to apply either L_z or one of the ladder operators to s or p atomic orbital. Conveniently the p-type real orbitals are given by the eigenstates of the above operators. Using a shorthand notation $|m_l\rangle$ where m_l is the magnetic quantum number, the p orbitals are

$$\begin{aligned} |x\rangle &= \frac{1}{\sqrt{2}}(|1\rangle + |-1\rangle) \\ |y\rangle &= \frac{1}{\mathrm{i}\sqrt{2}}(|1\rangle - |-1\rangle) \\ |z\rangle &= |0\rangle\,. \end{aligned} \tag{5.17}$$

Recall that L_z operating on $|m_l\rangle$ gives the eigenvalue $\hbar m_l$ but state $|m_l\rangle$ is not an eigenstate of $L_\pm$. However, $L_\pm$ acting on the state produces an eigenstate of L_z with $L_\pm\,|m_l\rangle = \hbar\sqrt{(l \mp m_l)(l \pm m_l + 1)}\,|m_l \pm 1\rangle$.

Finally, it's time to calculate the matrix elements. In order to do this, let's sketch a prototype which instantaneously shows the required operator. The matrix element between arbitrary eigenstates of the operator is

$$\begin{aligned} &\begin{pmatrix} \langle m_l,\uparrow| & \langle m_l,\downarrow| \end{pmatrix} \mathbf{L}\cdot\mathbf{S} \begin{pmatrix} |m_l',\uparrow\rangle \\ |m_l',\downarrow\rangle \end{pmatrix} \\ &= \frac{\hbar}{2}\left(\langle m_l,\uparrow|\,L_z\,|m_l',\uparrow\rangle + \langle m_l,\uparrow|\,L_-\,|m_l',\downarrow\rangle\right. \\ &\left. + \langle m_l,\downarrow|\,L_+\,|m_l',\uparrow\rangle - \langle m_l,\downarrow|\,L_z\,|m_l',\downarrow\rangle\right). \end{aligned} \tag{5.18}$$

We can already see that any matrix element involving s orbital vanishes. This is because atomic orbitals are orthogonal to each other. Also the expectation values of L_z and $L_\pm$ are zero for s orbital.

Including spin-orbit interaction to our Hamiltonian doubles the basis size. In effect the basis is $\{\mathrm{s}_1^\uparrow, \mathrm{p}_{x1}^\uparrow, \mathrm{p}_{y1}^\uparrow, \mathrm{p}_{z1}^\uparrow, \mathrm{s}_2^\uparrow, \mathrm{p}_{x2}^\uparrow, \mathrm{p}_{y2}^\uparrow, \mathrm{p}_{z2}^\uparrow$ + same for spin down$\}$ and we have a 16×16 Hamiltonian. Now we need to calculate all the spin-orbit interaction matrix elements between p orbitals. Hence there are 36 terms to be calculated. Actually most of these turn out to be zero and we can even use the Hermiticity of the Hamiltonian to reduce the number of calculations. Here are two examples of the calculations of the nonzero elements which there are twelve in total:

$$\begin{aligned}
\langle y_\uparrow \,|\, \mathbf{L}\cdot\mathbf{S} \,|\, x_\uparrow\rangle &= \langle y_\uparrow \,|\, L_z \,|\, x_\uparrow\rangle \\
&= -\frac{1}{2\mathrm{i}}(\langle 1| - \langle -1|)L_z(|1\rangle + |-1\rangle) \\
&= -\frac{\hbar}{2\mathrm{i}}(\langle 1\,|\,1\rangle - \langle 1\,|\,-1\rangle - \langle -1\,|\,1\rangle + \langle -1\,|\,-1\rangle) \\
&= -\frac{\hbar}{2\mathrm{i}}(1+1) \\
&= \mathrm{i}\hbar \\
\langle x_\uparrow \,|\, \mathbf{L}\cdot\mathbf{S} \,|\, x_\downarrow\rangle &= \langle x_\uparrow \,|\, L_- \,|\, z_\downarrow\rangle \\
&= \frac{1}{\sqrt{2}}(\langle 1| + \langle -1|)L_- \,|0\rangle \\
&= \hbar(\langle 1\,|\,-1\rangle + \langle -1\,|\,-1\rangle) \\
&= \hbar.
\end{aligned}$$

Each of the elements has a factor of $\hbar$ which we can dump into the strength parameter λ. Therefore the above elements are just i and 1, respectively. The matrices produced this way are

$$SO_{\uparrow\uparrow} = \lambda \begin{bmatrix} 0 & 0 & 0 & 0 \\ 0 & 0 & -i & 0 \\ 0 & i & 0 & 0 \\ 0 & 0 & 0 & 0 \end{bmatrix} \tag{5.19}$$

and

$$SO_{\uparrow\downarrow} = \lambda \begin{bmatrix} 0 & 0 & 0 & 0 \\ 0 & 0 & 0 & 1 \\ 0 & 0 & 0 & -i \\ 0 & 1 & -i & 0 \end{bmatrix} \tag{5.20}$$

where $SO_{\uparrow\uparrow}$ describes the interaction between spin up orbitals and $SO_{\uparrow\downarrow}$ between spin up orbitals and spin down orbitals.

Using these matrices the total Hamiltonian is

$$H = \begin{bmatrix} A + SO_{\uparrow\uparrow} & B & SO_{\uparrow\downarrow} & 0 \\ B' & A + SO_{\uparrow\uparrow} & 0 & SO_{\uparrow\downarrow} \\ SO_{\downarrow\uparrow} & 0 & A + SO_{\downarrow\downarrow} & B \\ 0 & SO_{\downarrow\uparrow} & B' & A + SO_{\downarrow\downarrow} \end{bmatrix} \tag{5.21}$$

where $SO_{\downarrow\uparrow} = SO'_{\uparrow\downarrow}$ and $SO_{\downarrow\downarrow} = SO'_{\uparrow\uparrow}$. The hopping elements give rise to a block diagonal matrix and spin-orbit interaction couples opposite spins to each other. Note also that the blocks due to the hopping and on-site terms corresponding to different spins are identical. Therefore the spin up and spin down bands would be degenerate. Now however, spin-orbit coupling directly lifts the degeneracy as the matrix $SO_{\uparrow\uparrow}$ describes the up spins whereas $SO_{\downarrow\downarrow}$ describes the down spins.

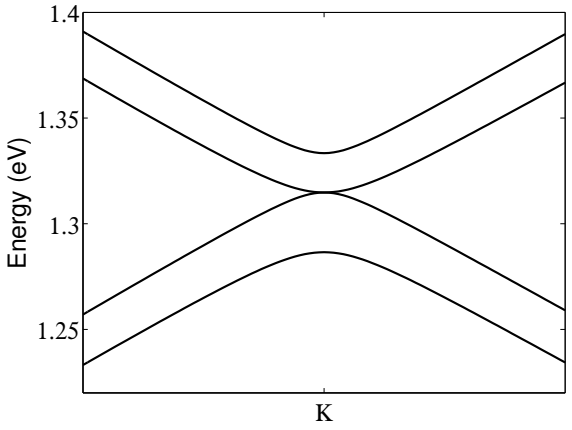

Figure 5.3: Effect of intra-atomic spin-orbit coupling near the K point.

Solving the eigenvalues of the Hamiltonian gives the dispersion relation presented in figure 5.3. The strength of spin-orbit interaction is 34 meV [15]. It is naturally a small perturbation which thus cannot be seen on full scale band plot such as figure 5.2. Nevertheless, we are mainly interested in what happens in the vicinity of the K point which is exactly what figure 5.3 tells us. As was discussed, the spin degeneracy is lifted which leads to a splitting of each band to two bands that follow the same dispersion. This in turn is simply the consequence of intra-atomic SOC being independent of $\mathbf{k}$. Most notably there still isn't a band gap as two of the bands shown cross each other. As a result the band structure is still qualitatively the same as was obtained from the bare hopping model. Therefore we now abandon the intra-atomic spin-orbit coupling and turn to study the effect of inter-atomic SOC.

5.2.2 Reduced Hamiltonian and inter-atomic coupling

The bands near the Fermi-energy in figure 5.2 have primarily p_z character. Since these bands are in the interesting energy range, we reduce the TB basis to contain only the p_z orbitals and set their on-site energy to zero. In effect the Fermi-energy lies now at zero electron volts with the size of the Hamiltonian being only 4×4. Now the next subject is to introduce inter-atomic spin-orbit interaction using this minimal basis and see how the electronic structure behaves at K point. The model presented here was first derived by Liu et al. [15]. Notably, it is a model designed specifically for silicene and so we will be using this constantly from now on.

The general Hamiltonian for the spin-orbit coupling requires relativistic derivation. Therefore one can use the Dirac equation instead of the Schrödinger equation to arrive at a Hamiltonian H_{so} describing spin-orbit interaction as

$$H_{so} \propto \nabla V \times \mathbf{p} \cdot \bar{\sigma} = -\mathbf{F} \times \mathbf{p} \cdot \bar{\sigma} \tag{5.22}$$

where $\mathbf{p}$ is momentum, $\bar{\sigma}$ is the vector of Pauli matrices (spin operator) and $\mathbf{F}$ is the force caused by potential. Note that this leads to equation 5.14 when the potential is the atomic potential.

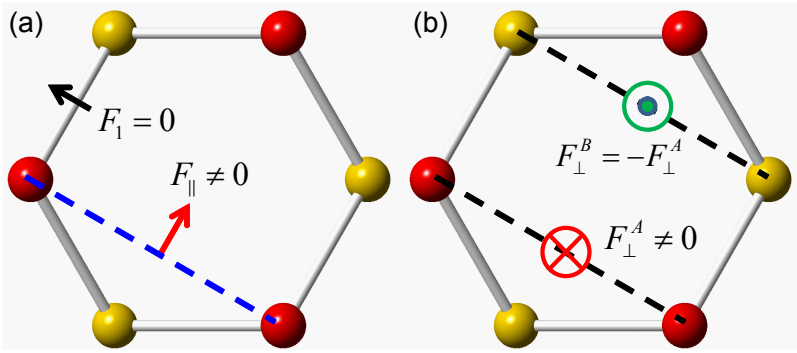

Figure 5.4: (a) Nearest neighbour SOC vanishes but next nearest SOC is nonzero from symmetry aspects. (b) Perpendicular force components are due to the nonplanar sublattices. [15].

Now, however, we look at a larger picture and take the whole crystal potential into account. First one should examine figure 2.2 showing the silicene structure. Any bond connecting nearest neighbours has other atoms symmetrically surrounding it. Therefore the average force along the bond due to each atomic potential gets cancelled out by an equal but opposite contribution from an atom at the other side of the bond. Hence the nearest-neighbour SOC vanishes.

On the other hand, there isn't such symmetry along a line between next nearest neighbours as indicated in figure 5.4 (a). At this point we should refer to figure (b) and yet again recall the buckled nature of silicene which causes the force to have

both parallel and perpendicular components. This is why we need to look at the different components separately.

First we analyze the component parallel with the silicene plane. We have the Hamiltonian

$$H_{so}^{\parallel} = \mathrm{i}\gamma_1(\mathbf{F}_{\parallel} \times \mathbf{d}_{ij}) \cdot \bar{\sigma} \tag{5.23}$$

where γ_1 is a parameter and $\mathbf{d}_{ij}$ is vector to the next nearest neighbour. Note that the next nearest neighbours belong to the same sublattice. Therefore they lie in the same plane and $\mathbf{d}_{ij}$ is parallel with the plane as well. As a result the cross product of $\mathbf{F}_{\parallel}$ and $\mathbf{d}_{ij}$ points perpendicular to the plane, i.e. to z-direction. In summary only the z-component of the dot product survives

$$H_{so}^{\parallel} = \mathrm{i}\frac{\lambda_{so}}{3\sqrt{3}}\nu_{ij}\sigma_z. \tag{5.24}$$

Here λ_{so} is the SOC strength for the parallel component, $\nu_{ij} = \frac{(\mathbf{d}_i \times \mathbf{d}_j)^z}{|(\mathbf{d}_i \times \mathbf{d}_j)^z|} = \pm 1$ and $\mathbf{d}_i$ and $\mathbf{d}_j$ are the two nearest bonds connecting the next nearest neighbour $\mathbf{d}_{ij}$. Note that there are six next nearest neighbours around any atom and therefore three positive and three negative terms with respect to ν_{ij}.

We can verify that the Hamiltonian 5.24 is Hermitian. The matrix element $H_{so}^{\parallel}(i,j)$ is proportional to $\mathrm{i}\nu_{ij}$ and since only ν changes for the transpose element, we get $H_{so}^{\parallel}(j,i) \propto \mathrm{i}\nu_{ji}$. As changing the vectors in ν only reverses its sign, we easily see the Hermiticity property of the Hamiltonian: $H_{so}^{\parallel}(j,i) = -\mathrm{i}\nu_{ij} = (\mathrm{i}\nu_{ij})^* = H_{so}^{\parallel}(i,j)^*$ where the common constants have been dropped from the equalities.

For the perpendicular component we want to switch the operators in the scalar triple product 5.22 to obtain

$$H_{so}^{\perp} = \mathrm{i}\gamma_2(\bar{\sigma} \times \hat{\mathbf{d}}_{ij}) \cdot \mathbf{F}_{\perp} \tag{5.25}$$

where $\hat{\mathbf{d}}_{ij} = \frac{\mathbf{d}_{ij}}{|\mathbf{d}_{ij}|}$, i.e. unit vector in the direction of $\mathbf{d}_{ij}$. This time we know that $\mathbf{F}_{\perp}$ points perpendicular to the plane and so only the z-component of the dot product is nonzero. In effect we pick only the z-component of the cross product to arrive at

$$H_{so}^{\perp} = \mathrm{i}\frac{2\lambda_R}{3}\mu_{ij}(\bar{\sigma} \times \hat{\mathbf{d}}_{ij})^z \tag{5.26}$$

where λ_R measures the strength of the perpendicular SOC component and μ_{ij} is 1 for A site and -1 for B site. This definition for μ_{ij} arises because $\mathbf{F}_{\perp}$ points up for A-A interaction due to the B atoms lying lower. Similarly the A atoms are behind the perpendicular force component for the B-B interaction and $\mathbf{F}_{\perp}$ points down in this case. The magnitudes of the force components are naturally equal between these cases due to symmetry. [15].

Let's again verify the Hermiticity of the Hamiltonian 5.26. From equation 5.33 we see that the matrix element is proportional to $H_{so}^{\perp}(i\uparrow, j\downarrow) \propto \mathrm{i}(\bar{\sigma}\times\hat{\mathbf{d}}_{ij})^z = \mathrm{i}(d_y+\mathrm{i}d_x) = -d_x+\mathrm{i}d_y$. Then looking at the transpose element and ignoring irrelevant constants, we obtain $H_{so}^{\perp}(j\downarrow, i\uparrow) = \mathrm{i}(\bar{\sigma}\times\hat{\mathbf{d}}_{ji})^z = \mathrm{i}(-d_y+\mathrm{i}d_x) = -d_x-\mathrm{i}d_y = (-d_x+\mathrm{i}d_y)^* = H_{so}^{\perp}(i\uparrow, j\downarrow)^*$. Hence the Hamiltonian is Hermitian as required.

To sum up, we have the total Hamiltonian

$$H = -t\sum_{\langle i,j\rangle\alpha} c_{i\alpha}^{\dagger}c_{j\alpha} + \mathrm{i}\frac{\lambda_{SO}}{3\sqrt{3}}\sum_{\langle\langle i,j\rangle\rangle\alpha\beta}\nu_{ij}c_{i\alpha}^{\dagger}\sigma_{\alpha\beta}^{z}c_{j\beta} - \mathrm{i}\frac{2}{3}\lambda_R\sum_{\langle\langle i,j\rangle\rangle\alpha\beta}\mu_{ij}c_{i\alpha}^{\dagger}(\bar{\sigma}\times\hat{\mathbf{d}}_{ij})_{\alpha\beta}^{z}c_{j\beta} \quad (5.27)$$

where the first term is the nearest-neighbour hopping Hamiltonian. The other two terms are the spin-orbit interaction corrections where $\langle\langle i,j\rangle\rangle$ indicates sum over next nearest neighbours and α, β are spin states. The second term is the effective SOC and the last term is called Rashba SOC. Next we derive how these terms are translated into matrix elements.

Effective spin-orbit coupling

Figure 5.5 depicts the six next nearest neighbours of atom A where the sign at each atom is the sign of ν_{ij}. The nearest neighbours are also presented in the figure to help determine these signs. Note also that the vector between next nearest neighbours is $\mathbf{a}_1$, $\mathbf{a}_2$ or the difference of these.

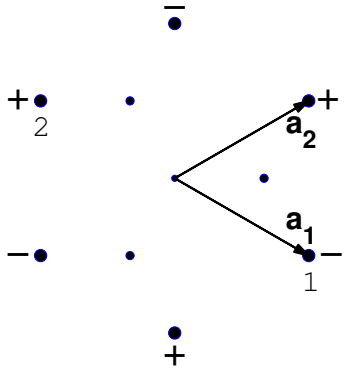

Figure 5.5: The closest neighbours of atom A. The value of ν_{ij} is marked with a plus or a minus sign.

Let's recall that the Pauli matrix is $\sigma_z = \begin{bmatrix} 1 & 0 \\ 0 & -1 \end{bmatrix}$. We can now look only at the spin up–spin up term and we have

$$H_{SOC}^{\uparrow\uparrow} = \mathrm{i}\frac{\lambda_{so}}{3\sqrt{3}}\sum_{1}^{6}\nu_{ij}\mathrm{e}^{\mathrm{i}\mathbf{k}\cdot\mathbf{d}_{ij}} \quad (5.28)$$

where the phase factor has also been explicitly written. If we now look only at the

pair of atoms 1 and 2 and ignore the common constants, we get

$$\begin{aligned}\nu_1 e^{i\mathbf{k}\cdot\mathbf{a}_1} + \nu_2 e^{-i\mathbf{k}\cdot\mathbf{a}_1} &= e^{-i\mathbf{k}\cdot\mathbf{a}_1} - e^{i\mathbf{k}\cdot\mathbf{a}_1} \\ &= \cos(\mathbf{k}\cdot\mathbf{a}_1) - i\sin(\mathbf{k}\cdot\mathbf{a}_1) - \cos(\mathbf{k}\cdot\mathbf{a}_1) - i\sin(\mathbf{k}\cdot\mathbf{a}_1) \\ &= -2i\sin(\mathbf{k}\cdot\mathbf{a}_1).\end{aligned} \tag{5.29}$$

The other two pairs give similar expressions so that in total we have the matrix element

$$\varepsilon_{so}^{A\uparrow}(\mathbf{k}) = \frac{2\lambda_{so}}{3\sqrt{3}}[\sin(\mathbf{k}\cdot\mathbf{a}_1) - \sin(\mathbf{k}\cdot\mathbf{a}_2) + \sin(\mathbf{k}\cdot(\mathbf{a}_2 - \mathbf{a}_1))]. \tag{5.30}$$

This is all we need to calculate since only the terms ν_{ij} change sign in the case of atom B. We can then readily say that $\varepsilon_{so}^{B\uparrow}(\mathbf{k}) = -\varepsilon_{so}^{A\uparrow}(\mathbf{k})$ and the terms change sign again for spin down.

Rashba spin-orbit coupling

The starting point of Rashba terms is

$$-i\frac{2\lambda_R}{3}\sum_1^6 \mu_{ij}(\bar{\sigma}\times\hat{\mathbf{d}}_{ij})^z_{\alpha\beta} e^{i\mathbf{k}\cdot\mathbf{d}_{ij}}. \tag{5.31}$$

We once again look at the A atoms ($\mu_{ij} = 1$) and take the atom pair 1 and 2. We have

$$\begin{aligned}&(\bar{\sigma}\times\hat{\mathbf{a}}_1)^z e^{i\mathbf{k}\cdot\mathbf{a}_1} - (\bar{\sigma}\times\hat{\mathbf{a}}_1)^z e^{-i\mathbf{k}\cdot\mathbf{a}_1} \\ &= a_{12}\cos(\mathbf{k}\cdot\mathbf{a}_1) + ia_{12}\sin(\mathbf{k}\cdot\mathbf{a}_1) - a_{12}\cos(\mathbf{k}\cdot\mathbf{a}_1) + ia_{12}\sin(\mathbf{k}\cdot\mathbf{a}_1) \\ &= 2ia_{12}\sin(\mathbf{k}\cdot\mathbf{a}_1)\end{aligned} \tag{5.32}$$

where $a_{12} = (\bar{\sigma}\times\hat{\mathbf{a}}_1)^z$. If we now sum up all the three pairs, we obtain an expression $\frac{4\lambda_R}{3}[a_{12}\sin(\mathbf{k}\cdot\mathbf{a}_1) + a_{34}\sin(\mathbf{k}\cdot\mathbf{a}_2) + a_{56}\sin(\mathbf{k}\cdot(\mathbf{a}_2 - \mathbf{a}_1))]$. Lastly we just need to work out the cross product in each term a.

The general form of the cross product is

$$(\bar{\sigma}\times\hat{\mathbf{d}}_{ij})^z = \sigma_x d_y - \sigma_y d_x = \begin{bmatrix} 0 & d_y + id_x \\ d_y - id_x & 0 \end{bmatrix} \tag{5.33}$$

where it should be noted that d_x and d_y are normalized coordinates. From figure 5.5 one can deduce that the coordinates of atom 1 are $\begin{pmatrix}\sin\frac{\pi}{3} & -\cos\frac{\pi}{3}\end{pmatrix}$ and so the spin up–spin down term is $a_{12}^{\uparrow\downarrow} = -\cos\frac{\pi}{3} + i\sin\frac{\pi}{3} = -e^{-i\frac{\pi}{3}}$. The other terms can be obtained in the same way which gives us the atom A matrix element

$$\varepsilon_R^{A\uparrow\downarrow}(\mathbf{k}) = \frac{4\lambda_R}{3}[-e^{-i\frac{\pi}{3}}\sin(\mathbf{k}\cdot\mathbf{a}_1) + e^{i\frac{\pi}{3}}\sin(\mathbf{k}\cdot\mathbf{a}_2) + \sin(\mathbf{k}\cdot(\mathbf{a}_2 - \mathbf{a}_1))]. \tag{5.34}$$

Furthermore it is once again easy to see that the same term for B atoms is just the same with a minus sign. It is also important to notice that the Rashba terms lie in the off-diagonal contrary to the effective SOC terms. In effect the term $\varepsilon_R^{A\downarrow\uparrow}$ should be complex conjugate of $\varepsilon_R^{A\uparrow\downarrow}$ to preserve Hermiticity. It is easily proven as only the terms a_{ij} change for the transpose element and equation 5.33 tells that $a_{ij}^{\downarrow\uparrow} = (a_{ij}^{\uparrow\downarrow})^*$. Since the imaginary unit doesn't exist anywhere else than in these terms, we can conclude that the Hermiticity is satisfied, $\varepsilon_R^{A\downarrow\uparrow} = (\varepsilon_R^{A\uparrow\downarrow})^*$.

Wave vector dependence of Hamiltonian matrix elements

Comparing the behaviours of SOC, Rashba and hopping terms as a function of wave vector is important to understand the features of the band structure. Most importantly we wish to see the difference at K (K') point to understand which terms affect the gap and why. Additionally symmetrical **k**-dependence, i.e. are the values at **k** and $-\mathbf{k}$ related to each other, is interesting to look for.

Without further ado, let's analyze SOC and Rashba terms in equations 5.30 and 5.34 which are plotted in figure 5.6. Hopping term $t(\mathbf{k})$ is also presented in figure (a). The path taken is from negative K point to positive K point through Γ, i.e. the center of the zone. The path continues from K point to K' point along the zone boundary. In effect we actually traverse through M point as well which is situated between K and K' point. Pay attention to the different nature of the terms. SOC lies on the diagonal of the Hamiltonian and it is therefore purely real. Rashba and hopping terms, however, are complex and so figures 5.6 (a) and (c) show both the real and imaginary parts.

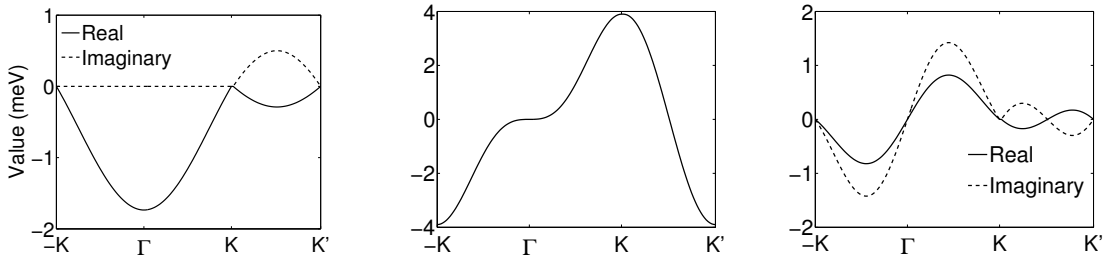

(a) Hopping (b) SOC (c) Rashba

Figure 5.6: Variation of different terms in the Hamiltonian.

Note that -K point is equivalent to K' point and so the values in each figure coincide at these two points. More important however is that the k-points along -K–Γ are negative whereas points along Γ–K are the same with positive sign. We see that the values for SOC and Rashba terms are equal in magnitude but have opposite signs when k-point changes sign. This can of course be easily seen from the

mathematical expressions as well. The hopping term on the contrary acts differently as there's no change of sign when k-point changes sign.

The behaviours of the terms differ in other ways as well. SOC peaks at K point whereas Rashba term has its maximum between Γ and K points, i.e. inside the Brillouin zone rather than at its boundary. There is also symmetry between the real and imaginary parts of Rashba term. The parts have the same sign inside the zone but opposite sign along the zone boundary.

Looking at the hopping term, it is clear that the bands cross at K point as hopping term vanishes there. Interestingly it can also be seen that the imaginary part is zero inside the Brillouin zone and only emerges at the zone boundary.

5.3 Effect of electric field and results

The last matter concerning bulk silicene is how electric field can be used to manipulate the band gap. After going through this we can determine how and why SOC and electric field affect the gap in liaison. For now we consider homogeneous electric field perpendicular to the silicene sheet.

This field has a simple effect. It merely changes the on-site energies of every p_z orbital. Furthermore, since the structure is buckled there is a potential difference between the two sublattices. In effect electric field tears the sublattices further apart. We now add this to the Hamiltonian in equation 5.27 to come up with

$$\begin{aligned} H = &- t\sum_{\langle i,j\rangle\alpha} c^\dagger_{i\alpha}c_{j\alpha} + \mathrm{i}\frac{\lambda_{SO}}{3\sqrt{3}}\sum_{\langle\langle i,j\rangle\rangle\alpha\beta}\nu_{ij}c^\dagger_{i\alpha}\sigma^z_{\alpha\beta}c_{j\beta} \\ &- \mathrm{i}\frac{2}{3}\lambda_R\sum_{\langle\langle i,j\rangle\rangle\alpha\beta}\mu_{ij}c^\dagger_{i\alpha}(\bar{\sigma}\times\hat{\mathbf{d}}_{ij})^z_{\alpha\beta}c_{j\beta} + \frac{\Delta}{2}\sum_{i\alpha}\mu_{ij}E_z c^\dagger_{i\alpha}c_{i\alpha}. \end{aligned} \tag{5.35}$$

The last term describes the electric field with μ_{ij} being the usual ± 1. E_z is the strength of the field and Δ is buckling parameter.

Let's ignore the Rashba term for now. We then have the Hamiltonian matrix

$$H = \begin{bmatrix} \varepsilon_0 + V + \varepsilon_{so}(\mathbf{k}) & t(\mathbf{k}) & 0 & 0 \\ t^*(\mathbf{k}) & \varepsilon_0 - V - \varepsilon_{so}(\mathbf{k}) & 0 & 0 \\ 0 & 0 & \varepsilon_0 + V - \varepsilon_{so}(\mathbf{k}) & t(\mathbf{k}) \\ 0 & 0 & t^*(\mathbf{k}) & \varepsilon - V + \varepsilon_{so}(\mathbf{k}) \end{bmatrix} \tag{5.36}$$

where ε_0 is the on-site energy (set to zero but included here for generality), $V = \frac{\Delta}{2}E_z$, $\varepsilon_{so} = \varepsilon^{A\uparrow}_{so}$ and $t(\mathbf{k})$ is the hopping term. If we don't have electric field, i.e. $V = 0$, the two blocks describing the opposite spins are identical. As a result the bands stay degenerate even if SOC is included. In addition, the eigenvalues of the matrix

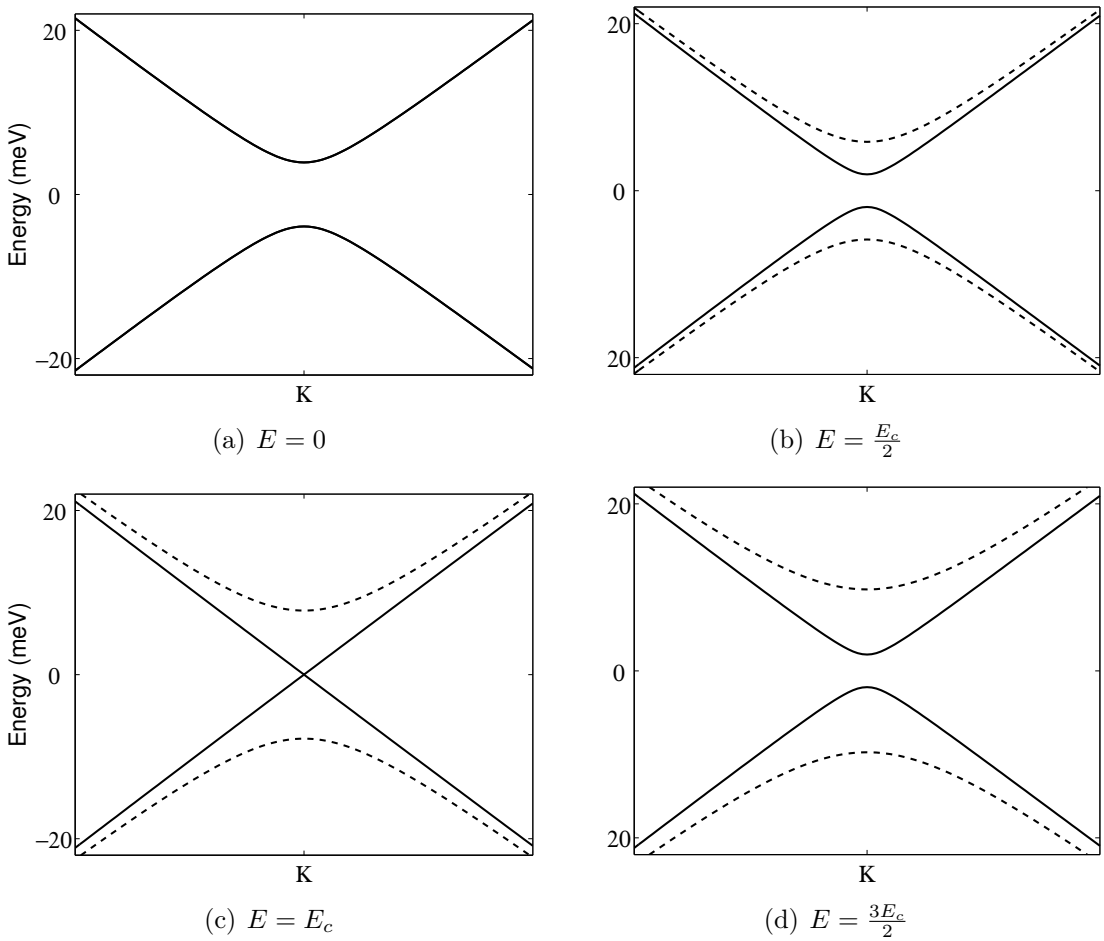

Figure 5.7: Variation of the band gap due to electric field. Spin up bands are drawn with solid lines, spin down bands with dashed lines. The script to reproduce the figures is presented in the appendix.

would be

$$\epsilon = \varepsilon_0 \pm \sqrt{\varepsilon_{so}^2(\mathbf{k}) - |t(\mathbf{k})|^2}. \tag{5.37}$$

Let's plot the band structure without electric field in figure 5.7 (a) which presents the dispersion near K point. Note that the figures have been obtained with Rashba term present. The values of the effective SOC and Rashba parameters are $\lambda_{so} = 3.9$ meV and $\lambda_R = 0.7$ meV. There are two notable features in this band plot: Firstly, we see that a band gap has developed due to the inter-atomic spin-orbit interaction. This is because SOC has nonzero value at K point. Secondly we notice that the bands are still degenerate which matches the discussion related to identical spin blocks.

We can also discern that the band gap is solely due to the effective SOC which is the main reason why we neglected Rashba terms in equation 5.36. This can be straightforwardly seen from figure 5.6 or by calculating the Rashba term (equation 5.34) at K point. Rashba term goes to zero whereas SOC term gives exactly λ_{so}

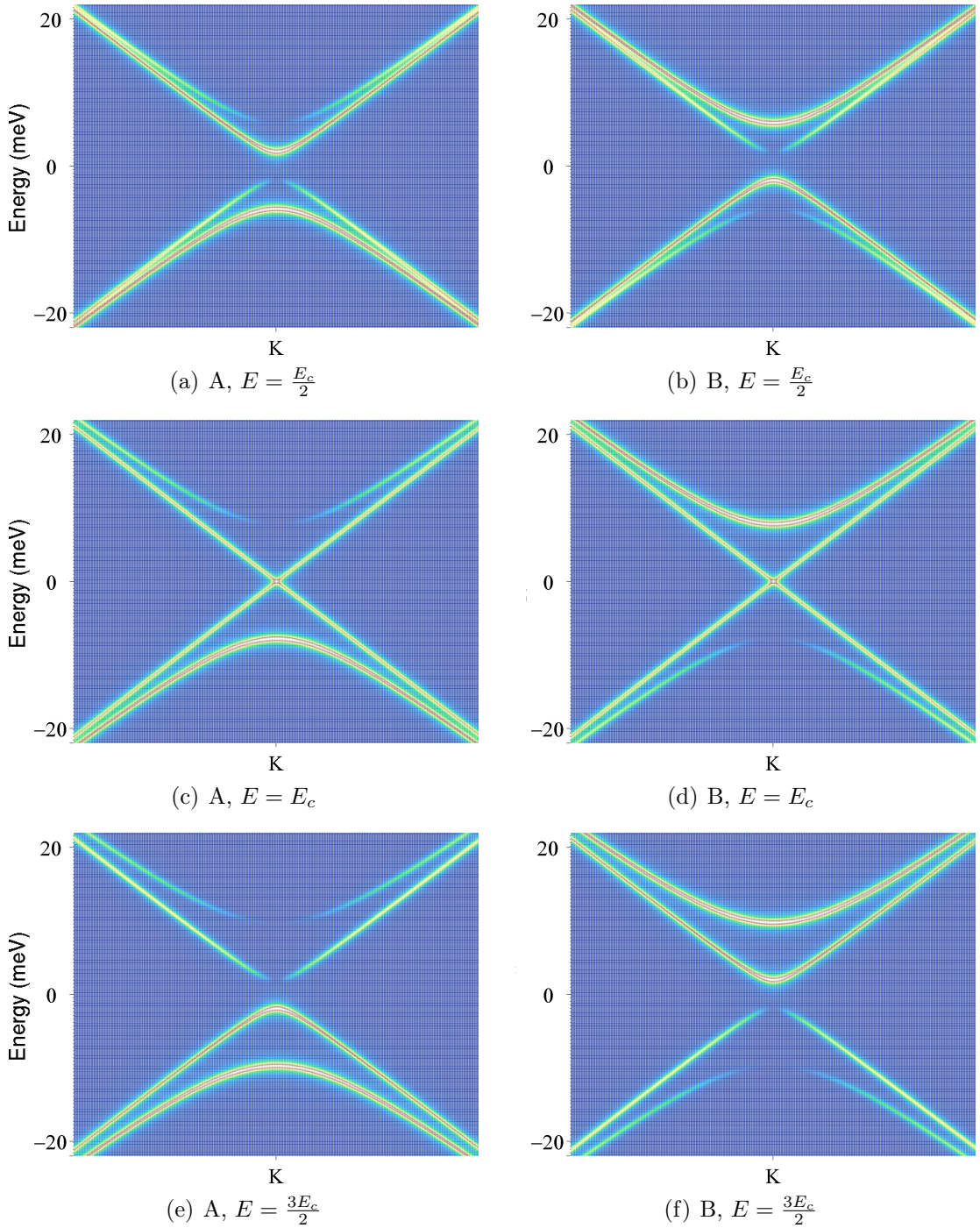

(a) A, $E = \frac{E_c}{2}$ (b) B, $E = \frac{E_c}{2}$

(c) A, $E = E_c$ (d) B, $E = E_c$

(e) A, $E = \frac{3E_c}{2}$ (f) B, $E = \frac{3E_c}{2}$

Figure 5.8: LDOS projections of atom A orbitals (left) and atom B (right).

at K point. It follows that the band gap is actually $2\varepsilon_{so}(\mathbf{K}) = 2\lambda_{so}$ giving a value of 7.8 meV. This is quite significant gap since it corresponds to 91 K temperature and is a great improvement from the SOC gap of graphene. Moreover it should be emphasized that this is an intrinsic gap that silicene possesses without any external manipulation.

Finally we can ask ourselves why the band gap develops exactly at K point.

To understand this we should again refer to figure 5.6 (b). SOC term reaches its maximum at K point (minimum at K' point) whereas the hopping term vanishes there causing the bands to cross. SOC is zero at Γ and M points which is the natural consequence of them being in the middle of K and K' points. Thus SOC term has to be zero at these points due to symmetry. In summary we see that SOC peaks where hopping term vanishes and vice versa. Hence conduction and valence bands can meet only at K point where, consequently, SOC drags them apart.

If we now let the electric field be nonzero in equation 5.36, we can immediately see that the spin blocks are inequivalent. Note that ignoring SOC altogether would again give us equivalent blocks meaning that the spin degeneracy is lifted only through the simultaneous interplay of both spin-orbit coupling and electric field. The eigenvalues in this case can be given independently for spins and they are

$$\begin{aligned} \epsilon_\uparrow &= \epsilon_0 \pm \sqrt{(V + \varepsilon_{so}(\mathbf{k}))^2 + |t(\mathbf{k})|^2} \\ \epsilon_\downarrow &= \varepsilon_0 \pm \sqrt{(V - \varepsilon_{so}(\mathbf{k}))^2 + |t(\mathbf{k})|^2}. \end{aligned} \tag{5.38}$$

Rashba interaction would of course alter the eigenvalues. It is however a small term even compared to effective SOC. More importantly though, Rashba SOC is zero at K point where this result gets interesting. The spin up gap is $2|V + \lambda_{so}|$ whereas spin down gap is $2|V - \lambda_{so}|$. Combining these we get $2|V + s_z\lambda_{so}|$ where $s_z = \pm 1$ for spin up (down). However, note that $\varepsilon_{so}(-\mathbf{k}) = -\varepsilon_{so}(\mathbf{k})$ as can be easily seen from equation 5.30. This means that the spins change roles at K' point which corresponds to -K point. In the end the band gap is

$$E_g = 2\left|\frac{\Delta}{2}E_z + \eta s_z \lambda_{so}\right| \tag{5.39}$$

where $\eta = \pm 1$ at K (K') point [6].

Equation 5.39 shows the development of the gap in the presence of an electric field. Figures 5.7 (b)–(d) demonstrates the effect where the solid lines depict spin up bands. Spin down bands are shown with dashed lines. First the gap decreases linearly as a function of E_z. At a critical electric field, E_c, the gap vanishes. When we further increase electric field, the gap opens up again and grows linearly. The critical point is easily seen to be

$$E_c = \frac{2\lambda_{so}}{\Delta}. \tag{5.40}$$

Figure 5.7 (c) illustrates the closure of the gap. Note that the spin up bands cross whereas the spin down band exhibit a big gap at K point as indicated by equation 5.38. Also note that we get the same band structure at K' point except that the spin bands have switched, i.e. the spin down bands would cross at K' point.

Furthermore, we can also switch the bands with each other by reversing electric field. It is important aspect to understand that the K and K' points are inequivalent only in the presence of electric field. Without the field, bands are degenerate and so it is insignificant which spin band we are looking at.

Imagine now silicene in a perpendicular electric field. The strength of the field is E_c and so the gap is closed at each K and K' point. In a sufficiently low temperature the three K points would be occupied by spin up electrons at Fermi-energy whereas the three K' points would be occupied by spin down electrons. If we now could separate the different K valleys from each other, we would be able to have spin-filtered current. An application related to this has been proposed by Tsai et al. [32].

So far we have only made a distinction between spins. It is also informative to look at the contributions from different sublattices individually. Figure 5.8 continues where figure 5.7 left and shows LDOS projections of the total contributions from atom A and atom B.

The figures show a few important features. First we see that the bands are fully spin polarized only at the K point exactly. Spin polarization gradually diminishes with $\mathbf{k}$ deviating from K. We also see which bands have primarily atom A character and which come from atom B orbitals. These are opposite as could be expected.

Moreover, the most important aspect is revealed if we vary electric field strength and look at all the figures. It is seen that the weight from atom A shifts towards the other spin up band when going over the critical field. The same is seen for B atom. In effect we observe band inversion happening at the critical field. This is a characteristic result for topological insulators where band inversion happens when changing some parameter. This parameter is electric field for silicene. We will be coming back to this subject in the next chapter.

6. SILICENE NANORIBBONS

Reducing the dimensionality of bulk silicene, nanoribbons offer a different playing ground due to the finiteness of the system. We would expect the edges to have a very distinct electronic structure and magnetic properties from the rest of the ribbon. It would also be interesting to see whether nanoribbons introduce localized states which would be the consequence of the inequality between an atom at the edge and an atom in the bulk. In effect the edges play an essential part in applications as the lattice periodicity is broken.

First we take a look at what kind of nanoribbons we could have and how they differ from each other. This is followed by the band structures and how they change when we play with spin-orbit coupling and electric field. The last issue concerns a zigzag nanoribbon in an inhomogeneous electric field which creates an interface at the middle of the ribbon. This introduces interesting effects at the interface which are different from those at the edges.

6.1 Edge types

Like silicene is considered 2-dimensional, nanoribbons are 1-dimensional in the sense that they are periodic only in one dimension. A nanoribbon can be imagined to be cut from bulk silicene and so it has a certain width which has an important impact on its electronic structure. Additionally, the edges can have various shapes depending on how we cut the ribbon. Nevertheless, they can be formed as a combination of two fundamental edge types, namely zigzag and armchair edges.

Figure 6.1 visualizes these two cases. The armchair nanoribbon shows deep sags along the edge whereas the zigzag edge resembles gently sloping V letters. The figure also shows the unit cells for both cases. Since the structure is periodic only in one direction, the unit cell must encompass all the atoms along the full width of the ribbon. The unit cell height is marked with an a or z in each case.

There's also the issue of naming nanoribbons based on their width. For the armchair case we simply count how many atoms are side-by-side and come up with a shorthand notation 13-ASiNR which is the specific ribbon used as an example in the figure. In the zigzag case we count the number of zigzagging bonds and get 7-ZSiNR in the figure.

Note also that the number of orbitals in TB basis increases rapidly with the width.

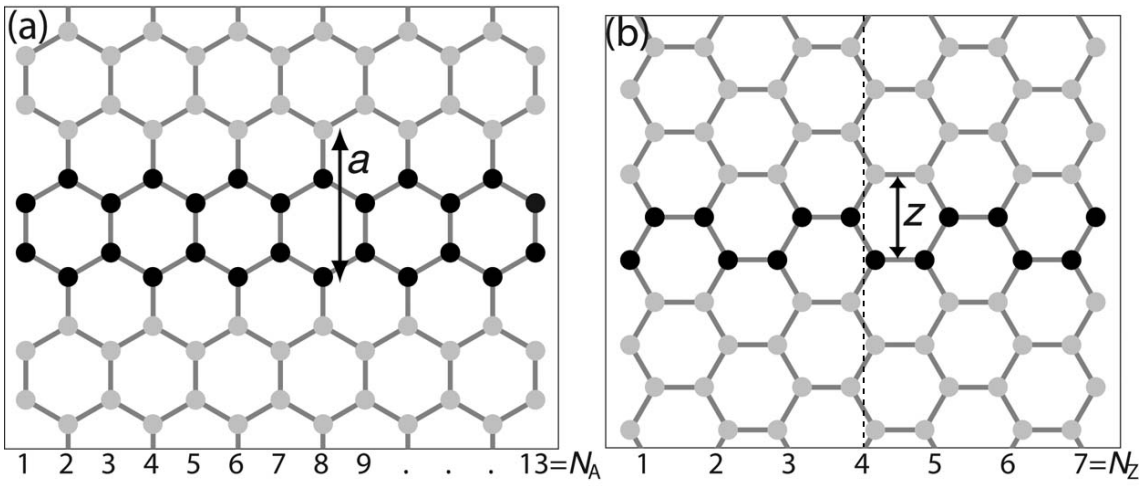

Figure 6.1: Labeling conventions and computational unit cell for (a) armchair (b) zigzag nanoribbon [12]. Electric field interface is drawn with a dashed line.

We need quite large matrices to model nanoribbons which can cause problems in the case of very wide ribbons. Thankfully most of the Hamiltonian matrix elements are zero, however, because we use nearest-neighbour hopping model. At most the interactions span over next nearest neighbours when we include SOC. So overall we have a lot of zeros in the Hamiltonian which we can take advantage of by using sparse matrices in the computational calculations.

6.2 Band structures

When forming the Hamiltonian for a nanoribbon, the edges need special treatment as some interactions are cut out. Keeping this in mind, we model both armchair and zigzag nanoribbons with effective SOC and Rashba terms included. Note that the spin-orbit coupling terms as well as hopping terms get split and are distributed to different positions in the Hamiltonian due to the reduced dimensionality. In effect the different terms in equations 5.30 and 5.34 are no longer summed but rather cut and distributed individually in the Hamiltonian.

The reciprocal space is also one-dimensional which further simplifies things. Figure 6.2 shows the band structure of 8-ZSiNR plotted from the center of Brillouin zone to the center of neighbouring zone at 4π which corresponds to 0. The band structure shown is characteristic to all zigzag ribbons regardless of width. As each orbital in the TB basis adds a new band, we have 16 bands in the figure. Increasing the width of the ribbon increases the number of bands which are closer and closer to each other effectively forming a continuum of states in infinity. However, qualitatively the band structure remains the same.

There are two things to point out in figure 6.2. First it should be emphasized that the effect of spin-orbit interaction cannot be seen at this scale so we are effectively

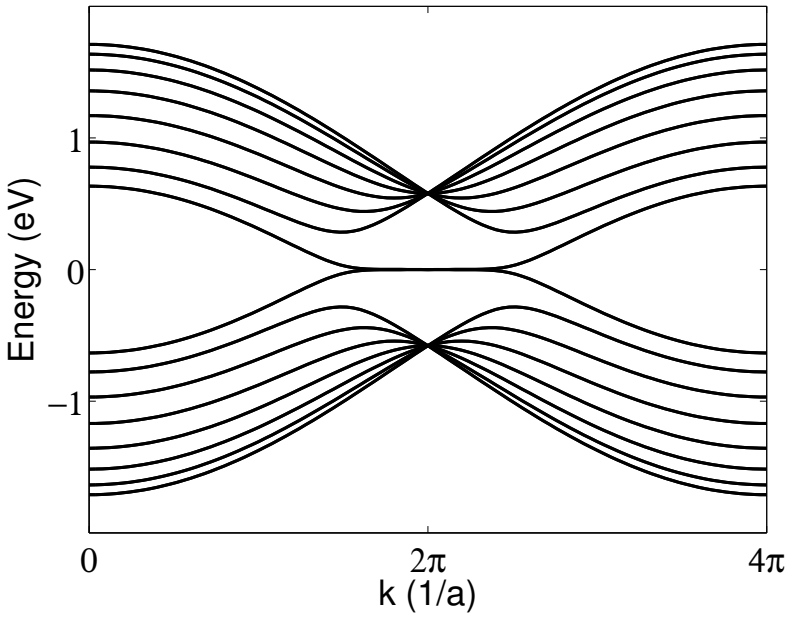

Figure 6.2: Band structure of 8-ZSiNR.

looking at the hopping model. The Fermi-energy lies at 0 eV where we see that the bands cross at the Brillouin zone boundary located at 2π. In effect zigzag nanoribbon is gapless analogously to bulk silicene.

Contradictory to zigzag ribbons, armchair ribbons are richer in features as the nature of the band structure depends on the ribbon width. For example, figure 6.3 shows the band structures of 8-ASiNR and 9-ASiNR. As one can surprisingly see,

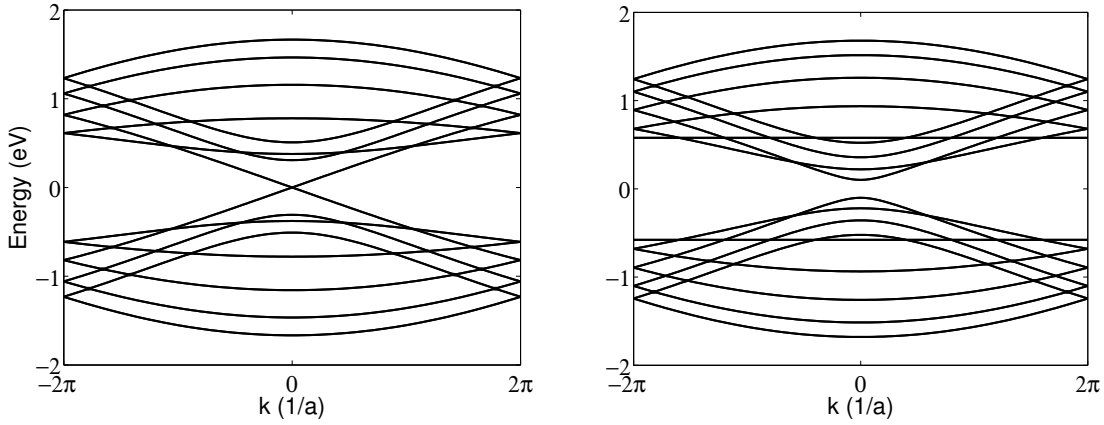

(a) 8-ASiNR is metallic

(b) 9-ASiNR is semiconducting

Figure 6.3: Band structures of two armchair nanoribbons.

the other ribbon is metallic whereas the other is semiconductor featuring a small band gap. This result is similar to what has been seen for graphene nanoribbons. Therefore, knowing this, we shouldn't be very surprised to see the same effect happen in silicene. In general TB calculations predict armchair nanoribbon to be metallic

when $N_A = 3p + 2$ and semiconducting when $N_A = 3p$ or $N_A = 3p + 1$ where p is integer.

Another clear feature is that the band gap (or crossing of the bands) occurs at the center of the Brillouin zone. This is a big difference compared to zigzag nanoribbons where the bands cross at the zone boundary. Now, however, we focus only on the zigzag geometry and zoom in at the zone boundary to see the effects of SOC and electric field.

6.2.1 Brillouin zone boundary

The Brillouin zone boundary is the most interesting area of the band plot since the bands cross there at Fermi-energy. Also spin-orbit interaction and electric field show their nature in this area. Figure 6.5 shows the zone boundary area in four different situations. This figure should be compared with figure 6.2 to get an idea how far from the zone boundary the plots stretch.

First figure 6.5 (a) shows only the results from the hopping model where we see that the bands remain degenerate exceedingly far from the boundary. Adding SOC to the model, we still don't get spin degeneracy lifted. Nonetheless, SOC separates the two bands and effectively removes their degeneracy. The system still remains gapless despite this.

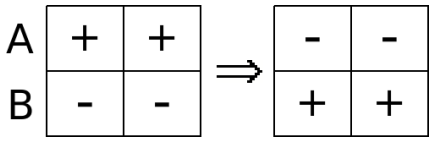

(a) Homogeneous electric field

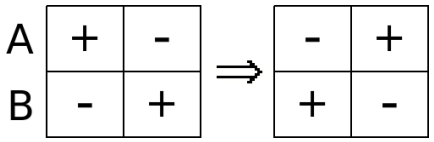

(b) Inhomogeneous field with equal strengths

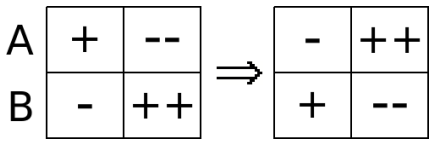

(c) Inhomogeneous field with unequal strengths

Figure 6.4: Mirror symmetries due to electric field. Left: initial circumstances. Right: Mirror image with A and B changing places.

When we put the ribbon in a homogeneous perpendicular electric field, we get

a similar result to the bulk silicene in that the spin bands are now separate, figure 6.5 (c). This also has the effect of developing a gap at the zone boundary. However, bands are still crossing some distance away from the boundary. This observation raises the question whether we can truly create a band gap by increasing electric field. This should drag the band crossing point further and further away from the boundary until the bands finally separate.

As it turns out, this is exactly what electric field does. We could now again define the critical electric field E_c where this separation happens. But alas, E_c depends on the width of the ribbon and so it differs from the critical field of bulk silicene.

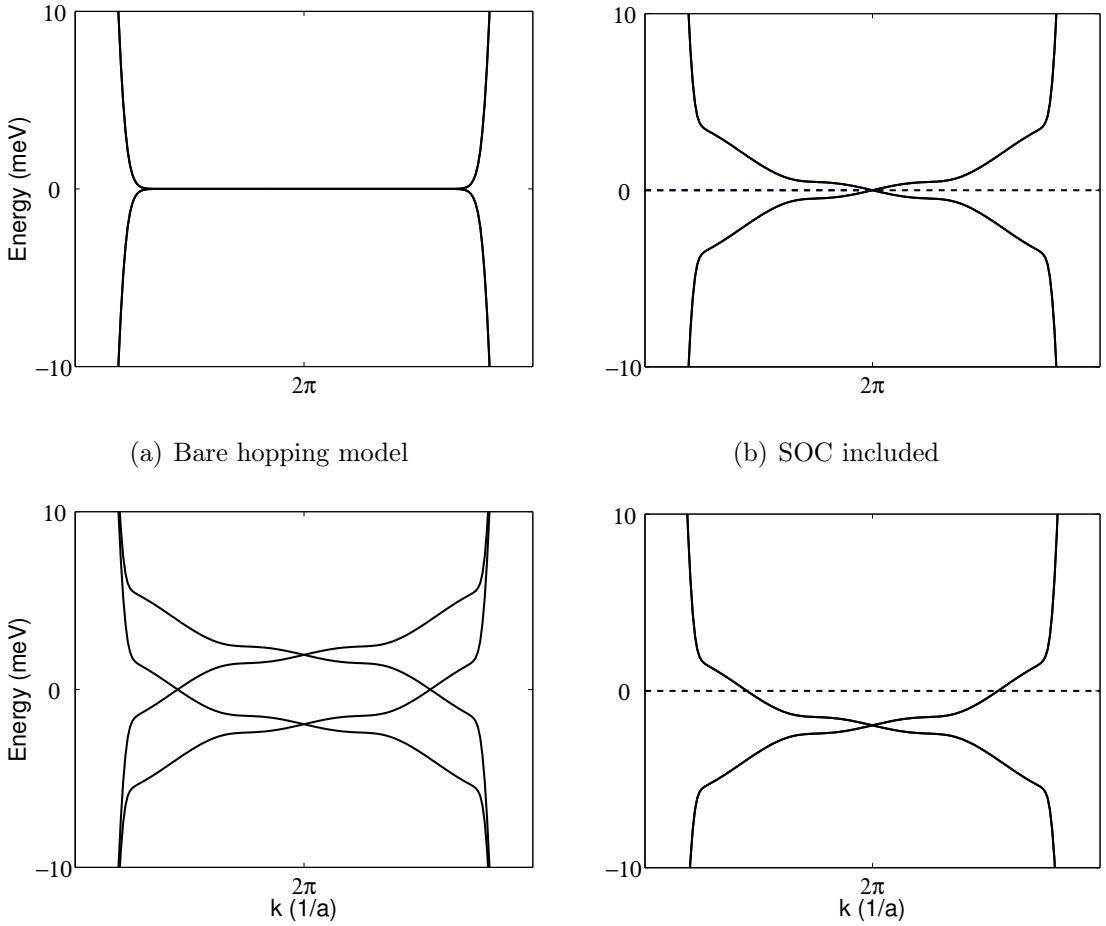

(a) Bare hopping model

(b) SOC included

(c) SOC with homogeneous electric field

(d) SOC with inhomogeneous electric field

Figure 6.5: The effect of various terms at the Brillouin zone boundary. Dashed line marks the Fermi-energy. 50-ZSiNR is used as example.

The last figure labeled 6.5 (d) involves inhomogeneous electric field perpendicular to the ribbon plane. More specifically we have put one half of the ribbon under homogeneous electric field $\mathbf{E}$ and the other half under electric field $-\mathbf{E}$, figure 6.1 (b). In effect their magnitudes are the same but directions are opposite. This creates an interface in the middle of the ribbon. Note that there are two different places

where to set the interface depending on ribbon width. It is however irrelevant which one we choose to use since electric field doesn't couple neighbouring sites.

Interestingly the effect of the setup is to only shift the bands in the energy scale. Figure 6.5 (d) should be compared with 6.5 (b) where only SOC is included. Notably also spin degeneracy is not lifted contrary to the case of homogeneous field. This is actually the consequence of additional mirror symmetry introduced by inhomogeneous field. Figure 6.4 sketches the situation where A atoms are in the upper row and B atoms lie at the lower row with the middle of the ribbon marked with a vertical line. In figure 6.4 (a) we have homogeneous electric field. It raises the on-site energies of A atoms (+) and lowers those of B atoms (-). This breaks the symmetry between the sublattices since after mirroring A and B the shifts in their on-site energies have reversed. Note that mirroring A and B is equivalent to changing the sign of electric field. In the case of inhomogeneous electric field, however, where the fields have equal magnitudes, half of the A atoms still have their on-sites raised and half have their on-sites lowered after mirroring. The system is therefore not changed in any way. In effect homogeneous field breaks mirror symmetry allowing spin eigenvalues to differ. Inhomogeneous field reintroduces the same kind of symmetry.

The spin degeneracy in figure 6.5 (d) is in fact only present when the fields on the different halves are equal in magnitude. When we let their strengths differ, mirror symmetry is once again removed (figure 6.4 (c)) and so is spin degeneracy. Note that electric field has no direct effect on spin. It rather separates A and B sublattices which causes splitting of the bands. Anyway, recall also that the effect of inhomogeneous electric field is that it allows us to shift the bands as we please.

We will focus more intensively on inhomogeneous electric field in section 6.3. Now however we should analyze the bands in real space and see how they are localized.

6.2.2 Localization of states

Comparing edge states to the states in the middle of the ribbon, let's call them bulk states, could reveal new important features. For this purpose we need the Green's function of the system from which we can calculate the local density of states for the edge atom and plot this projection in figure 6.6. Figure (a) shows the contribution from $p_z^{\uparrow}$ orbital and figure (b) from the spin down orbital. Electric field is not present here so the LDOS projections should be compared to figure 6.5 (b).

As can be immediately seen, contributions from opposite spins are different. Furthermore, even though the scale of the figure does not reveal it, we get few states outside the region shown in the figure so that the edge states are confined to a rather narrow window. In effect it seems that the flat bands around Brillouin zone boundary are actually purely edge states and they are even spin polarized. Remember also

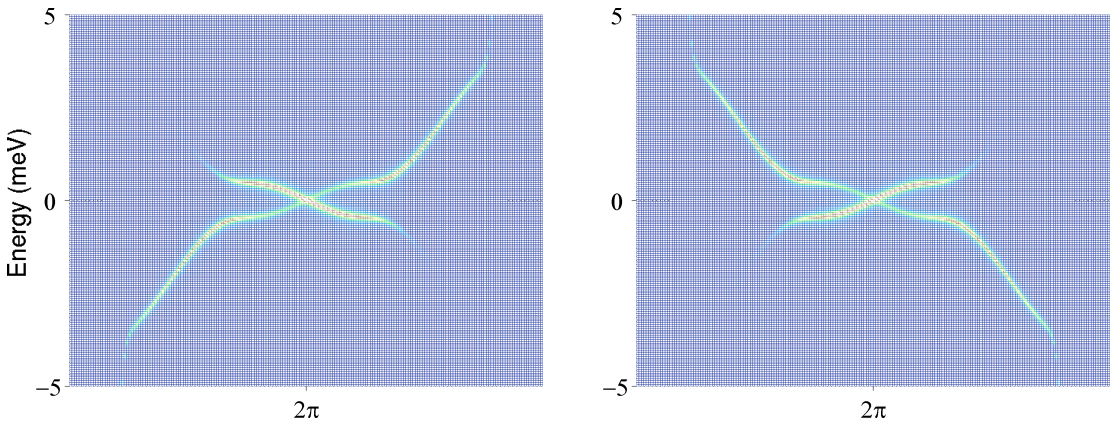

(a) Spin up (b) Spin down

Figure 6.6: LDOS contributions from spin up and spin down orbitals at the edge. The states show spin polarization. The figures are calculated for 50-ZSiNR.

that the ribbon has two edges and only the other is shown here. If we calculate the LDOS projections from the other edge too, we see the same result except that the spin contributions have reversed. This suggest that one band is up spin polarized (at least partly) on the left edge. The same band is then down spin polarized on the right edge.

However, we have not yet demonstrated that the flat bands come solely from the edges of the ribbon. We could now calculate LDOS projection in some bulk site in the same manner but actually the density of states diagrams in figure 6.7 will do also. The densities of states have been calculated with k-points ranging through the whole Brillouin zone and thus the figure tells us the overall picture how states are distributed.

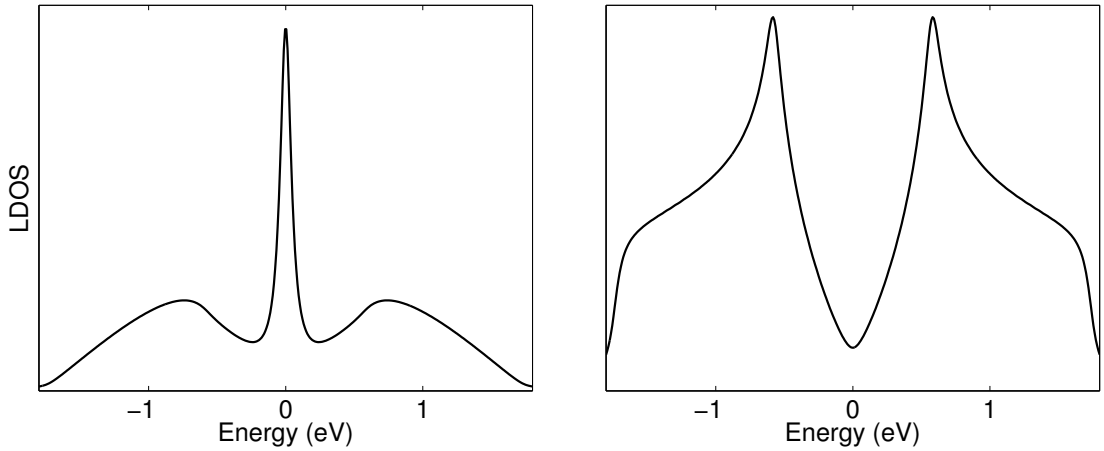

(a) Edge (b) Bulk

Figure 6.7: Density of states at the edge and in the bulk for 50-ZSiNR.

Figure 6.7 (a) shows DOS at the edge which is just as we would expect. DOS

is highly peaked around the Fermi-energy exactly where the flat bands are located. This confirms that there are very few states other than the flat bands at the edges of the ribbon. Figure 6.7 (b) on the contrary shows DOS at bulk site, i.e. in the middle of the ribbon. It is completely different as one could expect and peaks at about ± 0.6 eV. Most importantly, however, we see that there aren't practically any states at Fermi-energy proving that the flat bands are purely edge states. They are highly localized as the flat bands nearly disappear when traveling only couple of atoms away from the edge. This also leads to the fact that there exists a sizable bulk band gap as the flat bands are not present there. The edge states then lie in the bulk gap.

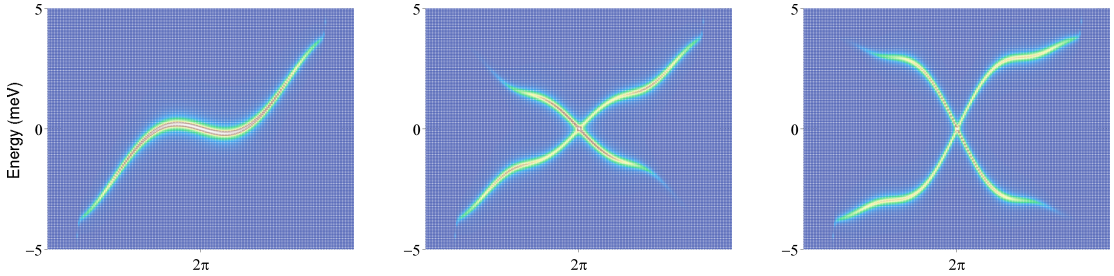

(a) $\lambda_R = 0$ (b) $\lambda_R = \frac{\lambda_{so}}{2}$ (c) $\lambda_R = \lambda_{so}$

Figure 6.8: Rashba spin-orbit coupling effect on edge states. Demonstration is for left edge and spin up.

Curiously the edge state bands are not purely spin polarized as the other bands always shows small polarization. This is in fact caused by Rashba interaction whose role is to mix spins. Figure 6.8 shows the edge states again for the left edge where we have arbitrarily chosen to look at spin up contribution. As can be seen, Rashba interaction enlarges the gap between bands around the boundary points. However, more important point here is how spin polarization is affected by Rashba SOC. Rashba SOC strength has been varied from zero (figure 6.8 (a)) to λ_{so} (figure 6.8 (c)). The real value of λ_R is about 18 % of λ_{so} so figures (b) and (c) are greatly exaggerated.

According to this demonstration we see that the edge state bands would indeed be purely spin polarized without Rashba term. This would correspond to a fully planar structure similar to graphene where A and B sublattices are coplanar. The effect of the buckling is then to mix spins so that edge states show some kind of mixing or hybridization. In the extreme case where Rashba strength equals SOC strength, there is very little spin polarization as spin down contribution would be almost identical to spin up.

Figure 6.7 (a) showed the combined LDOS from both spin orbital contributions. If we look at the peak more closely and calculate spin-resolved densities of states

separately for positive and negative k-points in the Brillouin zone, another surprising phenomenon emerges. It is most clearly presented by calculating spin polarization ρ from spin densities of states as

$$\rho = \frac{\rho_\uparrow - \rho_\downarrow}{\rho_\uparrow + \rho_\downarrow} \tag{6.1}$$

where equation 4.7 is put to use. Figure 6.9 shows the results of these calculations for the left edge.

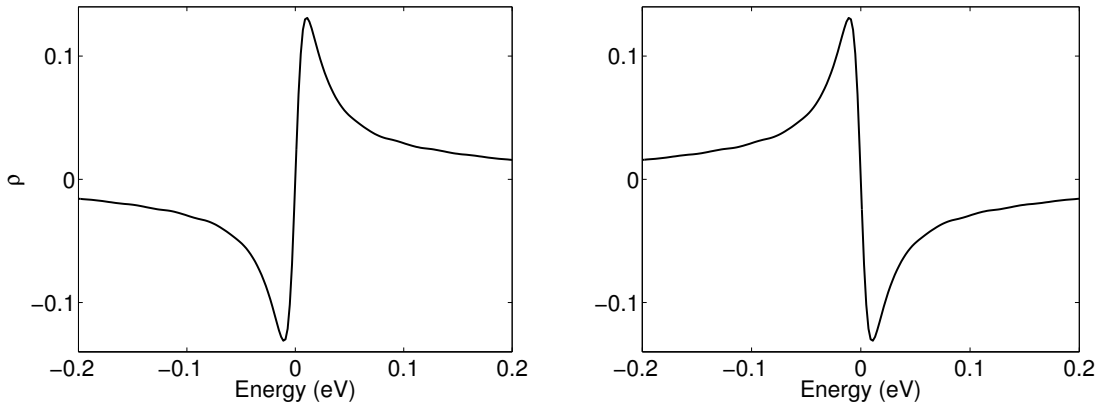

(a) Positive k-points (b) Negative k-points

Figure 6.9: Spin polarization at the edge site calculated for 50-ZSiNR.

If up and down spin densities of states were equal, we would see nothing in the figures. Instead, we can see peaks in the plots meaning that the difference is at its largest near the Fermi-energy. Positive peaks indicate an excess of up spin DOS whereas negative values indicate more down spin DOS. The peaks are also reversed when changing the sign of k-points indicating that spin and wave vector are coupled at the edge. In addition, spins once again change roles at the right edge. This is an important result as it resembles quantum spin hall effect met in topological insulators. In fact, combining spin and wave vector coupling with the knowledge of the localized edge states inside the bulk gap hints that we are dealing with a topological insulator. Indeed, Ezawa has shown this to be the case when electric field $|\mathbf{E}| < E_c$ [6]. At the critical field there occurs a phase transition from topological insulator to a band insulator which is easily understood since the edge states do not connect valence bands to conduction bands when $|\mathbf{E}| > E_c$.

6.3 Interfaced system

Finally we apply inhomogeneous electric field to silicene as described previously. The interface of the two fields in the middle of the ribbon is now interesting as it could show somehow localized effects like the edges. First however we extend the

nanoribbon and use 100-ZSiNR to ensure that the interface and the edges do not interact and distort the results.

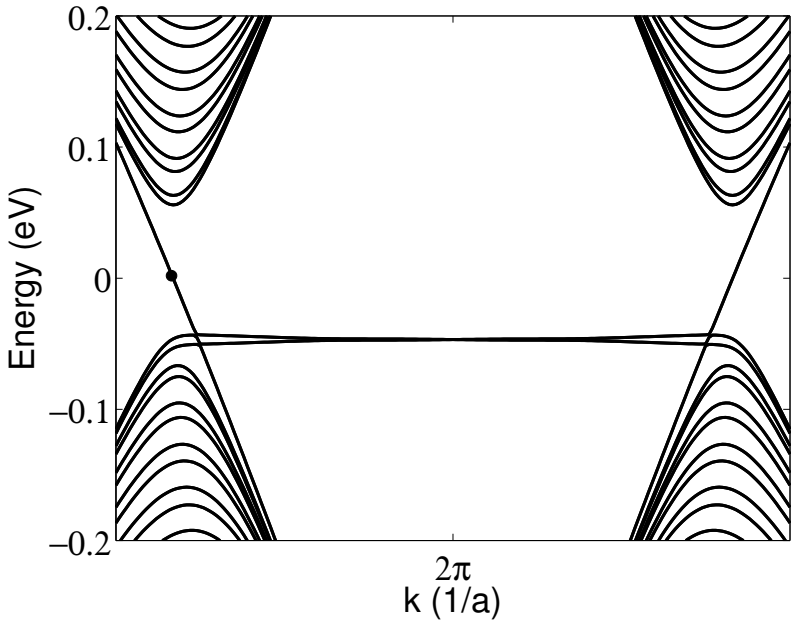

Figure 6.10: Band structure of 100-ZSiNR under inhomogeneous electric field of $12E_c$.

Figure 6.10 shows the band structure around Brillouin zone boundary for a rather strong field $|\mathbf{E}| = 12E_c$. We use the bulk critical field as a reference unit. Note that the electric field doesn't destroy the edge states or alter them in any way other than shifting them downwards. In effect the edge states don't go over the gap anymore. Instead we have bands with high dispersion connecting the conduction and valence bands.

Next we calculate LDOS projection at the interface. We also choose a site between the interface and edge to be compared with the interface states. These are shown in figure 6.11 where (a), (c) and (e) visualize LDOS far from the interface for various values of electric field. Figures (b), (d) and (f) show LDOS exactly at the interface site.

Figures 6.11 (a) and (b) show local densities of states when electric field is not present and so we do not even have any interface. This would imply that the two sites in the middle of the ribbon and one closer to the edge are more or less equivalent. This is as one would expect. Recall that the flat bands are present only at the edges of the ribbon and so they are not seen in these LDOS projections.

Figures 6.11 (c) and (d) show the situation when electric field is $6E_c$. Now we notice that the interface site has shifted its weight towards the steep bands crossing the gap. The other site further away from the interface has done the opposite: the bands with high dispersion have begun to vanish. Pay also attention to that the steep bands are not continuous here as there is a kink of some sort where the edge

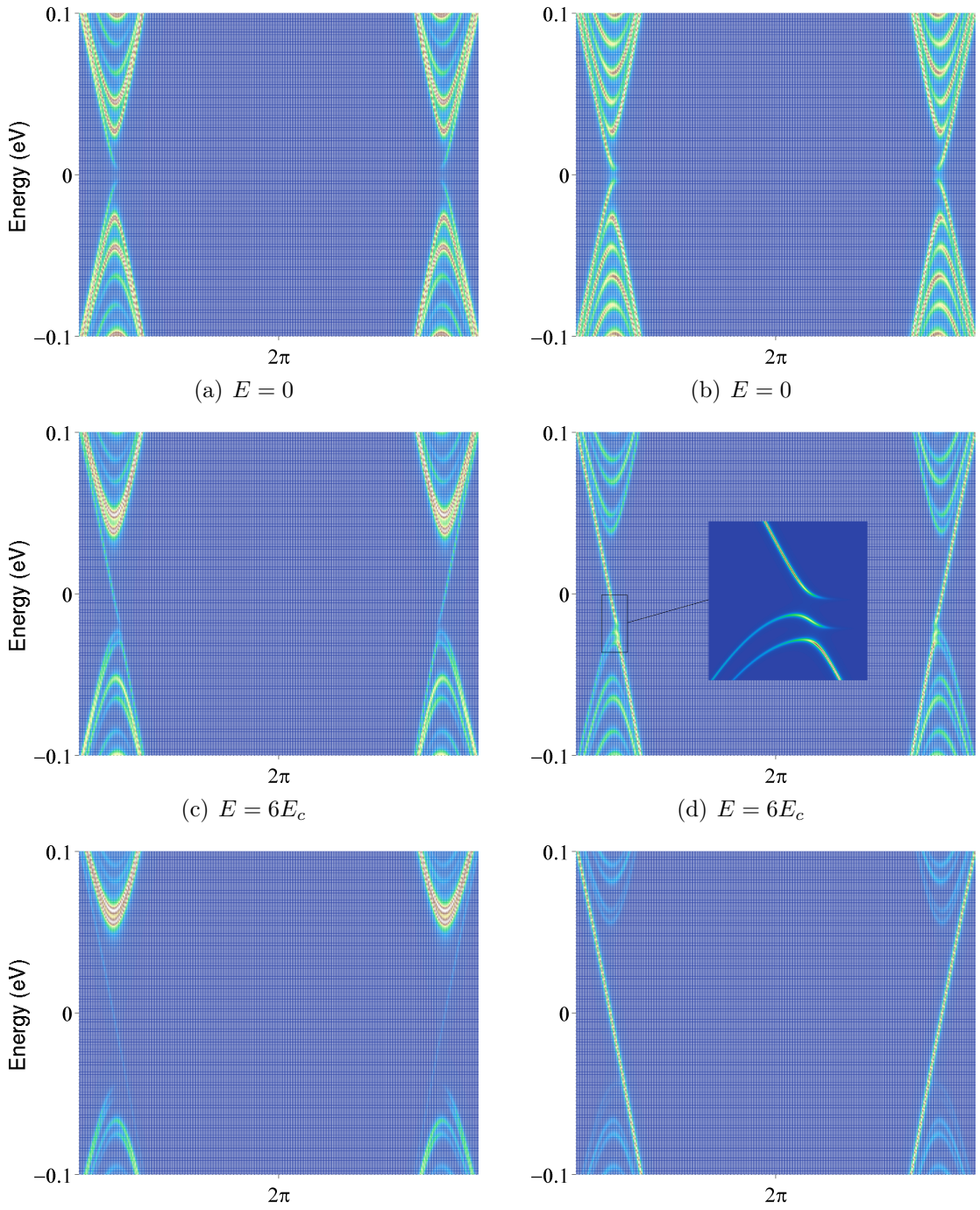

(a) $E = 0$ (b) $E = 0$

(c) $E = 6E_c$ (d) $E = 6E_c$

(e) $E = 12E_c$ (f) $E = 12E_c$

Figure 6.11: LDOS projections at two distinct sites of 100-ZSINR under inhomogeneous electric field. Left: site between interface and edge. Right: interface site.

states begin.

Finally in figure 6.11 (e) we see that the bands crossing the gap have basically vanished. They are now very strongly present at the interface site in figure (f). Also these interface bands are now continuous. This requires roughly the field $12E_c$ as presented in the figures.

In summary, bands crossing the gap localize near the interface when electric field is increased. Furthermore it becomes evident that the bands are not spin polarized when we calculate spin-resolved LDOS projections. This is the opposite of the edge states which show spin polarization. Also pay heed to the fact that the bands which localize at the interface are present in the whole ribbon (except at the edges) when electric field is zero. Therefore the effect of inhomogeneous electric field is very clear: it localizes the bands at the interface. It has no effect on the edge states other than shifting them away from the bulk gap.

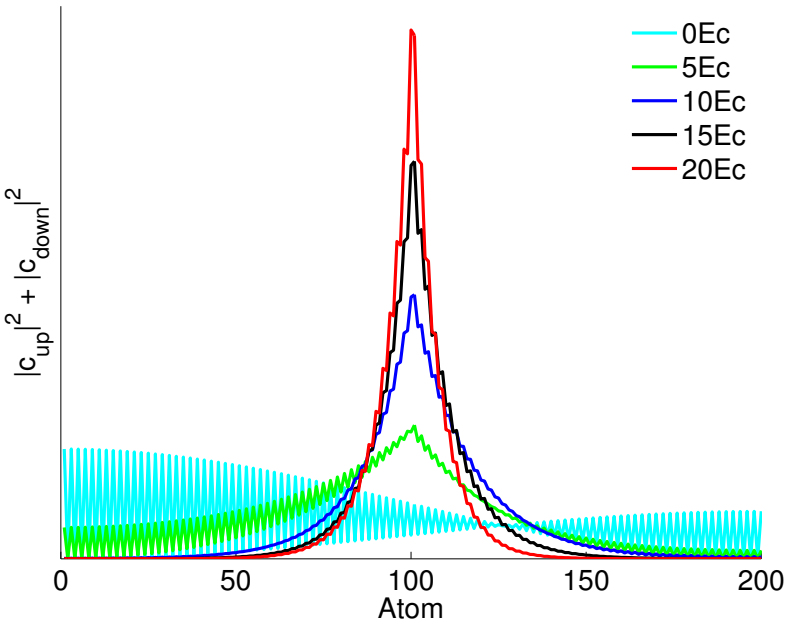

Figure 6.12: Localization of interface state as a function of electric field.

An obvious question would be how the localization behaves in real space as a function of electric field. To study this we have calculated the sum of spectral weights of both spin up and spin down orbitals (the numerator in equation 4.5) at every site in the ribbon at a specific k-point. The chosen point is marked with a dot in figure 6.10. This one k-point should represent any point along the interface band equally well.

Figure 6.12 indicates the nature of the localization. Atoms 0 and 200 are at the edges whereas the interface is located between atoms 100 and 101. At zero field the band is divided along the whole ribbon. The abrupt oscillation of the curve is due to the A and B sites which have different contributions. Also because of the same reason the curve is not symmetrical with respect to the interface. However, recall that the interface bands are spin degenerate. Repeating the calculation for the other degenerate band would lead to a diagram which is a mirror image of figure 6.12 and so the sum of these two would yield a symmetrical plot.

More importantly though we see that the localization strengthens with increasing

electric field. This is of course as one would expect. Nevertheless, the figure indicates a continuous change rather than some critical field where we would get a jump in the localization plot. The system also requires a fairly high electric field, about 10 E_c, to achieve strongly localized interface states.

7. CONCLUSIONS

The discussion on silicene's substrates states that some substrate is always needed and it is not possible to make freestanding silicene. Despite this we have ignored the effect of substrate and studied only independent sheet of silicene. However, the current knowledge of substrates is summarized in the following.

Thus far only three substrates have been experimentally found. These are (111)-oriented silver surface, (0001)-oriented zirconium diboride and (111)-oriented iridium. Ag(111) is not a good choice for any application because it destroys the Dirac cone in silicene. A study based on DFT calculations suggest that a much better candidate is h-BN [17]. This still requires experimental proof. In general the search of suitable substrates should be leaned towards solutions where the interaction between the substrate and silicene preserve silicene's properties, especially the Dirac cone.

In this thesis, silicene has been studied with tight-binding calculations. We have shown how spin-orbit coupling and electric field affect the electronic structure of silicene. As spin-orbit interaction is an intrinsic feature and therefore a fixed parameter, particular focus has been on electric field which can be externally tuned. Research on the matter has led to three main points.

Firstly, due to the buckled structure of silicene, spin-orbit interaction has both parallel (effective SOC term) and perpendicular (Rashba term) component with respect to the silicene plane. The intrinsic band gap at K and K' points in the Brillouin zone is caused solely by SOC. The size of band gap is several milli-electron volts which is unaffected by Rashba interaction as it vanishes at K (K') point.

By applying perpendicular electric field we can tune the band gap. First the gap diminishes linearly with increasing field. At a critical point the gap is closed after which it again starts to grow by further increasing electric field strength. Furthermore, the field also splits spin-degeneracy in such a way that the gap is between spin up bands at K point and between spin down bands at K' point.

Easy tuning of the band gap by electric field offers a convenient way to implement on and off states as required by e.g. transistors. However, the intrinsic gap is still rather small and so ways to further increase it are worth studying. In addition, the inequivalence of K and K' points allows us, in principle, to separate spin-currents.

Secondly, we have shown the existence of spin-polarized edge states lying in the

bulk gap in zigzag silicene nanoribbons. The edge states are highly localized at the edges of the ribbon with spin-polarization reversing between the edges. In addition, electron's spin is coupled to the direction of its motion at the edges showing the existence of quantum spin hall effect. As a conclusion we have seen silicene to be a topological insulator. However, this is only true when electric field strength does not exceed the critical point where band gap closes. By going over the critical field silicene becomes a trivial band insulator.

Thirdly we have placed silicene under inhomogeneous electric field such that the fields on separate halves have equal strengths but opposite signs. In effect this creates an interface in the middle of the ribbon. We have seen the building up of interface states with increasing electric field. With a high enough electric field the edge states no longer reside in the bulk gap. This causes a situation where the interface states alone go over the gap. This suggests a change in the nature of the material where initially the bulk is insulating and the edges conduct electricity. Under inhomogeneous electric field we see a change of conductance to the bulk with localization depending on the field strength. However, high localization requires rather strong fields. Also the localization of interface states still remains wide when compared to the edge states.

The system still requires more work. Possible further studies could include different geometry, for example armchair edges or a combination of armchair and zigzag. Also various defects could have a surprising impact and these could be studied with or without electric field. Furthermore, the combination of magnetic field and electric field should be worth studying.

REFERENCES

[1] Xing-Tao An, Yan-Yang Zhang, Jian-Jun Liu, and Shu-Shen Li. Quantum spin Hall effect induced by electric field in silicene. *Applied Physics Letters*, 102, 2013.

[2] Lan Chen, Baojie Feng, and Kehui Wu. Observation of a possible superconducting gap in silicene on Ag(111) surface. *Applied Physics Letters*, 102, 2013.

[3] Bruno Dlubak, Marie-Blandine Martin, Cyrile Deranlot, Bernard Servet, Stéphane Xavier, Richard Mattana, Mike Sprinkle, Claire Berger, Walt A. De Heer, Frédéric Petroff, Abdelmadjid Anane, Pierre Seneor, and Albert Fert. Higly efficient spin transport in epitaxial graphene on SiC. *Nature Physics*, 8(7):557–561, 2012.

[4] N. D. Drummond, V. Zólyomi, and V. I. Fal'ko. Electrically tunable band gap in silicene. *Physical Review B*, 85:075423, Feb 2012.

[5] E. Durgun, S. Tongay, and S. Ciraci. Silicon and III-V compound nanotubes: structural and electronic properties. Eprint, 2005. `arxiv.org/pdf/cond-mat/0505263`.

[6] Motohiko Ezawa. A topological insulator and helical zero mode in silicene under an inhomogeneous electric field. *New Journal of Physics*, 14, March 2012.

[7] Antoine Fleurence, Rainer Friedlein, Taisuke Ozaki, Hiroyuki Kawai, Ying Wang, and Yukiko Yamada-Takamura. Experimental evidence for epitaxial silicene on diboride thin films. *Physical Review Letters*, 108:245501, Jun 2012.

[8] Yunfei Gao, Y.J. Kubo, Chia-Ching Lin, Zhihong Chen, and J. Appenzeller. Optimized spin relaxation length in few layer graphene at room temperature. In *Electron Devices Meeting (IEDM), 2012 IEEE International*, pages 4.4.1–4.4.4, 2012.

[9] Stephen Gasiorowicz. *Quantum Physics*. John Wiley & Sons, third edition, 2003.

[10] Zhi-Xin Guo, Shinnosuke Furuya, Jun ichi Iwata, and Atsushi Oshiyama. Absence of Dirac electrons in silicene on Ag(111) surfaces. *Journal of the Physical Society of Japan*, 82(6):063714, 2013.

[11] Gian G. Guzmán-Verri and L. C. Lew Yan Voon. Electronic structure of silicon-based nanostructures. *Physical Review B*, 76:075131, Aug 2007.

[12] Y. Hancock, A. Uppstu, K. Saloriutta, A. Harju, and M. J. Puska. Generalized tight-binding transport model for graphene nanoribbon-based systems. *Physical Review B*, 81:245402, Jun 2010.

[13] H. Şahin, S. Cahangirov, M. Topsakal, E. Bekaroglu, E. Akturk, R. T. Senger, and S. Ciraci. Monolayer honeycomb structures of group-IV elements and III-V binary compounds: First-principles calculations. *Physical Review B*, 80:155453, Oct 2009.

[14] Boubekeur Lalmi, Hamid Oughaddou, Hanna Enriquez, Abdelkader Kara, Sébastien Vizzini, Bénidicte Ealet, and Bernard Aufray. Epitaxial growth of a silicene sheet. *Applied Physics Letters*, 97, 2010.

[15] Cheng-Cheng Liu, Hua Jiang, and Yugui Yao. Low-energy effective Hamiltonian involving spin-orbit coupling in silicene and two-dimensional germanium and tin. *Physical Review B*, 84:195430, Nov 2011.

[16] Feng Liu, Cheng-Cheng Liu, Kehui Wu, Fan Yang, and Yugui Yao. D+id' chiral superconductivity in bilayer silicene. Eprint, Sep 2012. `http://arxiv.org/abs/1208.5596v2`.

[17] Hongsheng Liu, Junfeng Gao, and Jijun Zhao. Silicene on substrates: A way to preserve or tune its electronic properties. *The Journal of Physical Chemistry*, 117:10353–10359, 2013.

[18] Lei Meng, Yeliang Wang, Lizhi Zhang, Shixuan Du, Rongting Wu, Linfei Li, Yi Zhang, Geng Li, Haitao Zhou, Werner A. Hofer, and Hong-Jun Gao. Buckled silicene formation on Ir(111). *Nano Letters*, 13:685–690, 2013.

[19] R. R. Nair, I.-L. Tsai, M. Sepioni, O. Lehtinen, J. Keinonen, A. V. Krasheninnikov, A. H. Castro Neto, M. I. Katsnelson, A. K. Geim, and I. V. Grigorieva. Dual origin of defect magnetism in graphene and its reversible switching by molecular doping. *Nature Communications*, 4(2010), 2013.

[20] Jouko Nieminen. Theory for picoscale scanning tunneling microscopy. In Klaus D. Sattler, editor, *Fundamentals of Picoscience*. CRC Press, 2013. To appear September 2013.

[21] M. Ali Omar. *Elementary solid state physics*. Addison-Wesley Pub. Co., 1975.

[22] Sami Paavilainen. *Geometric and electronic properties of adsorbate-substrate systems modelled with density-matrix tight-binding method*. PhD thesis, Tampere University of Technology, 2002.

[23] D. A. Papaconstantopoulos and M. J. Mehl. The Slater-Koster tight-binding method: A computationally efficient and accurate approach. *Journal of Physics: Condensed Matter*, 15, 2003.

[24] L. Petersen and P. Hedegård. A simple tight-binding model of spin-orbit splitting of sp-derived surface states. *Surface Science*, 459(1–2):49 – 56, 2000.

[25] Ruge Quhe, Ruixiang Fei, Qihang Liu, Jiaxin Zheng, Hong Li, Chengyong Xu, Zeyuan Ni, Yangyang Wang, Dapeng Yu, Zhengxiang Gao, and Jing Lu. Tunable and sizable band gap in silicene by surface adsorption. *Scientific Reports*, 2, 2012.

[26] Karri Saloriutta. *Electron transport in graphene nanostructures*. PhD thesis, Aalto University, 2013.

[27] J. C. Slater and G. F. Koster. Simplified LCAO method for the periodic potential problem. *Physical Review*, 94:1498–1524, Jun 1954.

[28] Adrian P. Sutton. *Electronic structure of materials*. Oxford University Press, 1993.

[29] Kyozaburo Takeda and Kenji Shiraishi. Theoretical possibility of stage corrugation in Si and Ge analogs of graphite. *Physical Review B*, 50:14916–14922, Nov 1994.

[30] *Nobelprize.org*. Nobel Media AB 2013. The Nobel Prize in Physics 2010 - Advanced Information. `http://www.nobelprize.org/nobel_prizes/physics/laureates/2010/advanced.html`, Jul 2013.

[31] Georgios A. Tritsaris, Efthimios Kaxiras, Sheng Meng, and Enge Wang. Adsorption and diffusion of lithium on layered silicon for Li-ion storage. *Nano Letters*, 13:2258–2263, 2013.

[32] Wei-Feng Tsai, Cheng-Yi Huang, Tay-Rong Chang, Hsin Lin, Horng-Tay Jeng, and A. Bansil. Gated silicene as a tunable source of nearly 100% spin-polarized electrons. *Nature Communications*, 4, 2013.

[33] P. Vogl, Harold P. Hjalmarson, and John D. Dow. A semi-empirical tight-binding theory of the electronic structure of semiconductors. *Journal of Physics and Chemistry of Solids*, 44(5):365 – 378, 1983.

[34] Patrick Vogt, Paola De Padova, Claudio Quaresima, Jose Avila, Emmanouil Frantzeskakis, Maria Carmen Asensio, Andrea Resta, Bénédicte Ealet, and Guy Le Lay. Silicene: Compelling experimental evidence for graphenelike two-dimensional silicon. *Physical Review Letters*, 108:155501, Apr 2012.

[35] Yun-Peng Wang and Hai-Ping Cheng. Does silicene on Ag(111) have a Dirac cone? Eprint, 2013. http://arxiv.org/abs/1302.5759.

[36] Chengyong Xu, Guangfu Luo, Qihang Liu, Jiaxin Zheng, Zhimeng Zhang, Shigeru Nagase, Zhengxiang Gao, and Jing Lu. Giant magnetoresistance in silicene nanoribbons. *Nanoscale*, 4:3111–3117, 2012.

[37] Wei Yu, Huaqing Xie, Xiaoping Wang, and Xinwei Wang. Significant thermal conductivity enhancement for nanofluids containing graphene nanosheets. *Physics Letters A*, 375(10):1323 – 1328, 2011.

[38] J. M. Ziman. *Elements of advanced quantum theory.* Cambridge University Press, 1969.

A. APPENDIX

The Matlab script below shows the code which calculates bulk silicene band structure in the vicinity of K point. By setting the variable Ez to zero in the script, one obtains figure 5.7 (a). Similarly figures (b)–(d) are obtained by playing with Ez.

```
% This code sample calculates silicene band structure
% in the vicinity of K point.

% Main function
function silicene
%------------------ Adjust these parameters at will ------------------%
points = 101; % Measures the number of k-points

% Electric field strength
% Critical point Ec = 0.0169
Ez = 0.0169;
%---------------------------------------------------------------------%

[R,a,a1,a2,onsite,lambda_SO,lambda_R,eigenvalues] = initialize(points);
[k,ticks,labels] = kpoints(a,points);

% Gather eigenvalues at every k-point
for index = 1:size(k,2)
    % Phase factors for each of the three neighbours.
    phase = zeros(3,1);
    for i = 1:3
        phase(i) = exp(1i*dot(k(:,index),R(:,i)));
    end
    % Hopping integrals
    hop = 0;
    for i = 1:3
        hop = hop + hopping(R(:,i))*phase(i);
    end

    % Inter-atomic SOC
    eff_SOC = 2*lambda_SO/(3*sqrt(3)) * (sin(a1*k(:,index))
              - sin(a2*k(:,index)) + sin((a2-a1)*k(:,index)));

    % Rashba SOC
    p = exp(1i*pi/3);
```

```
    rashba = 4*lambda_R/3 * (-1/p*sin(a1*k(:,index))
               + p*sin(a2*k(:,index)) + sin((a2-a1)*k(:,index)));

    % Electric field
    EF = 0.23076 * Ez * diag([-1 1 -1 1]);

    % Hamiltonian in the basis {pz1_up, pz2_up, pz1_down, pz2_down}
    H = [onsite+eff_SOC  hop              rashba           0;
         hop'            onsite-eff_SOC   0                -rashba;
         conj(rashba)    0                onsite-eff_SOC   hop(1);
         0               conj(-rashba)    hop'             onsite+eff_SOC]
         + EF;

    eigenvalues(index,:) = eig(H);
end

plot_bands(eigenvalues,ticks,labels);

%******************************************************%
%******************************************************%
function [R,a,a1,a2,onsite,lambda_SO,lambda_R,eigenvalues]
         = initialize(points)
% On-site energy
onsite = 0;

lambda_SO = 3.9*10^-3; % Inter-atomic SOC strength
lambda_R = 0.7*10^-3; % Rashba SOC strength

% Atomic coordinates in the unit cell
coordinates = [4.45714 0 0; % B
               2.22857 0 0.46152]; % A

% Initialize space for eigenvalues, 4 is basis size
eigenvalues = zeros(2*points,4);

% Lattice constant and vectors
a = 3.86;
a1 = a/2*[sqrt(3),-1,0];
a2 = a/2*[sqrt(3),1,0];

% Vectors to nearest neighbours
R1 = coordinates(2,:)-coordinates(1,:);
R2 = R1+a1;
R3 = R1+a2;
R = [R1' R2' R3'];

%******************************************************%
```

```
83 %*********************************************************%
84 % Construct k-points near K point
85 function [k,ticks,labels] = kpoints(a,points)
86 d = 0.01; % How far to travel from K point
87 % Go towards gamma point
88 x1 = linspace((1-d)*2*pi/(sqrt(3)*a), 2*pi/(sqrt(3)*a), points);
89 y1 = linspace((1-d)*2*pi/(3*a), 2*pi/(3*a), points);
90 % Go towards M point
91 x2 = linspace(2*pi/(sqrt(3)*a), (1-d)*2*pi/(sqrt(3)*a), points);
92 y2 = linspace(2*pi/(3*a), (1+d)*2*pi/(3*a), points);
93 k = [x1 x2; y1 y2 ; zeros(1,2*points)];
94 ticks = points;
95 labels = {'K'};
96
97 %*********************************************************%
98 %*********************************************************%
99 function [hop] = hopping(vector)
100 % Hopping parameters
101 Vpp_sigma = 2.72;
102 Vpp_pii = -0.72;
103
104 n = dot(vector,[0 0 1])/norm(vector); % Direction cosine
105 hop = n^2*Vpp_sigma+(1-n^2)*Vpp_pii;
106
107 %*********************************************************%
108 %*********************************************************%
109 function plot_bands(eigenvalues,ticks,labels)
110 figure;
111 hold on;
112 for i=1:size(eigenvalues,2)
113     plot(eigenvalues(:,i),'linewidth',2);
114 end
115 hold off;
116 box on;
117 set(gca,'fontsize',23);
118 ylabel('Energy (eV)');
119 set(gca,'XTick',ticks);
120 set(gca,'XTickLabel',labels,'FontName','Symbol');
121 xlim([1 length(eigenvalues)]);
122 ylim([-1 1]*0.022);
```